

# The structural dynamics of macropinosome formation and PI3-kinase-mediated sealing revealed by lattice lightsheet microscopy

**Shayne Quinn**

South Dakota School of Mines and Technology

**Lu Huang**

South Dakota State University

**Jason Kerkvliet**

South Dakota State University

**Joel Swanson**

University of Michigan-Ann Arbor <https://orcid.org/0000-0003-0900-8212>

**Steve Smith**

South Dakota School of Mines and Technology

**Adam Hoppe**

South Dakota State University <https://orcid.org/0000-0003-4180-0840>

**Robert Anderson**

South Dakota School of Mines and Technology

**Natalie Thiex**

South Dakota State University

**Brandon Scott** (✉ [brandon.scott@sdsmt.edu](mailto:brandon.scott@sdsmt.edu))

South Dakota School of Mines and Technology <https://orcid.org/0000-0002-1950-0748>

---

## Article

**Keywords:** microscopy, lattice lightsheet microscopy, phosphatidylinositol 3-kinase (PI3K)

**Posted Date:** December 28th, 2020

**DOI:** <https://doi.org/10.21203/rs.3.rs-121499/v1>

**License:**  This work is licensed under a Creative Commons Attribution 4.0 International License.

[Read Full License](#)

---

**Version of Record:** A version of this preprint was published at Nature Communications on August 10th, 2021. See the published version at <https://doi.org/10.1038/s41467-021-25187-1>.



1 The structural dynamics of macropinosome formation and PI3-kinase-mediated  
2 sealing revealed by lattice lightsheet microscopy

3

4

5 Shayne E. Quinn<sup>1,2</sup>, Lu Huang<sup>3,4</sup>, Jason G. Kerkvliet<sup>4,5</sup>, Joel A. Swanson<sup>6</sup>, Steve Smith<sup>1,2</sup>, Adam D. Hoppe<sup>4,5</sup>,  
6 Robert B. Anderson<sup>1,2</sup>, Natalie W. Thiex<sup>3,4\*</sup> Brandon L. Scott<sup>1,2\*</sup>

7 1 South Dakota School of Mines and Technology (South Dakota Mines), Nanoscience and Nanoengineering, Rapid  
8 City, SD. 2 BioSNTR, South Dakota Mines, Rapid City, SD. 3 South Dakota State University (SDSU), Department of  
9 Biology and Microbiology, Brookings, SD. 4 BioSNTR, SDSU, Brookings, SD. 5 SDSU, Department of Chemistry and  
10 Biochemistry, Brookings, SD. 6 University of Michigan, Department of Microbiology and Immunology, Ann Arbor, MI.

11 \* Co-corresponding authors: natalie.thiex@sdstate.edu, brandon.scott@sdsmt.edu

12

## 13 **Abstract**

14 Macropinosomes are formed by shaping actin-rich plasma membrane ruffles into large intracellular  
15 organelles in a phosphatidylinositol 3-kinase (PI3K)-coordinated manner. Here, we utilize lattice lightsheet  
16 microscopy and image visualization methods to map the three-dimensional structure and dynamics of  
17 macropinosome formation relative to PI3K activity. We show that multiple ruffling morphologies produce  
18 macropinosomes and that the majority form through non-specific collisions of adjacent PI3K-rich ruffles.  
19 By combining multiple volumetric representations of the plasma membrane structure and PI3K products,  
20 we show that PI3K activity begins early throughout the entire ruffle volume and continues to increase  
21 until peak activity concentrates at the base of the ruffle after the macropinosome closes. Additionally,  
22 areas of the plasma membrane rich in ruffling had increased PI3K activity and produced many  
23 macropinosomes of various sizes. Pharmacologic inhibition of PI3K activity had little effect on the rate and  
24 morphology of membrane ruffling, demonstrating that early production of 3'-phosphoinositides within  
25 ruffles plays a minor role in regulating their morphology. However, 3'-phosphoinositides are critical for the  
26 fusogenic activity that seals ruffles into macropinosomes. Taken together these data indicate that local  
27 PI3K activity is amplified in ruffles and serves as a priming mechanism for closure and sealing of ruffles  
28 into macropinosomes.

29

## 30 **Introduction**

31 Macropinocytosis, or “cell drinking,” is a form of clathrin-independent endocytosis that results in the non-  
32 specific uptake of large volumes of extracellular fluid and solutes. This central macrophage function  
33 enables immune surveillance, clearing of debris, and sampling of the local environment for the presence  
34 of pathogen- or damage-associated molecular patterns, cytokines, growth factors, nutrients, and other  
35 soluble cues<sup>1-6</sup>. Macropinosomes also serve as platforms to integrate this diverse information and to  
36 activate a variety of signaling pathways<sup>7-10</sup>. The major macrophage growth factor, colony-stimulating  
37 factor-1 (CSF-1), stimulates macropinocytosis and contributes to ligand-dependent modulation of CSF-1  
38 receptor signaling<sup>9</sup>. Additionally, cytokines such as CXCL12, and the bacterial cell wall component  
39 lipopolysaccharide (LPS) acutely stimulate macropinocytosis<sup>5,11,12</sup>.

40

41 Construction of a macropinosome proceeds through autonomous, ligand-independent plasma membrane  
42 extensions known as ruffles, which are driven by actin polymerization and require the phosphorylation  
43 and dephosphorylation of the different signaling phospholipids<sup>13,14</sup>. The closely related process of solid  
44 particle uptake known as phagocytosis has been hypothesized to use the shape of the particle as a  
45 template for the structure of the phagosome<sup>15,16</sup>. In contrast, the fusion of ruffles into macropinosomes  
46 do not have a structural framework to use as a template. This has resulted in various proposed closing  
47 mechanisms including a ‘purse string’ closure of circular dorsal ruffles<sup>13</sup>, closure at the distal tips of  
48 ruffles<sup>17</sup>, and more recently closure following actin tentpole crossing<sup>12</sup>. Regardless, these proposed  
49 mechanisms result in an organelle derived from the plasma membrane filled with the extracellular  
50 medium<sup>18</sup>. The production of 3' phosphoinositides by PI 3-kinase (PI3K) is required to generate isolated

51 patches of phosphatidylinositol 3,4,5-triphosphate (PIP<sub>3</sub>) on the plasma membrane<sup>3,19</sup>, and the sequential  
52 breakdown of PIP<sub>3</sub> into PI(3,4)P<sub>2</sub> and ultimately PI is necessary for successful macropinosome formation<sup>20</sup>.  
53 Previous ratiometric imaging has shown that PIP<sub>3</sub> concentration peaks after ruffle circularization<sup>21-23</sup>.  
54 Additionally, PI3K inhibitors, including LY294002, have demonstrated that PI3K activity is only required for  
55 macropinosome closure, but not ruffling<sup>24</sup>. This dynamic lipid microenvironment impacts the localization  
56 of downstream effector molecules driving actin polymerization and ruffle growth into macropinosomes<sup>22</sup>  
57 . However, it is only in protozoa, *i.e.*, *Dictyostelium*, that the spatial signaling coordination in the 3D ruffle  
58 volume during macropinocytosis has been well described<sup>19</sup>; it remains unclear how these events are  
59 spatially coordinated in metazoan cells<sup>25</sup>. The precise membrane dynamics of macropinocytosis and the  
60 spatial coordination of PI3K in forming ruffles remains unclear because of the low spatial and temporal  
61 resolution of previous microscopy approaches. Recently, high-resolution imaging of macropinocytosis in  
62 macrophage-like cell lines indicates that the prior models of macropinocytosis may need to be  
63 reconsidered<sup>12</sup>.

64 Here, we employ the powerful three-dimensional (3D) imaging capabilities of lattice lightsheet  
65 microscopy<sup>26</sup> (LLSM) and volumetric image analysis to create high-resolution movies of plasma membrane  
66 dynamics and PI3K activity during ruffling and macropinocytosis. The images and movies we present  
67 advance our understanding of the spatial dynamics of membrane ruffling and the morphologies that lead  
68 to macropinosomes, as well as the spatial distribution of PI3K activity during macropinocytosis. Our results  
69 show that the majority of macropinosomes form by non-specific collisions of adjacent PI3K-rich ruffles.  
70 We show that PI3K activity is present at the earliest stages of ruffle extensions and is highly localized to  
71 the bottom of ruffles after the membrane has closed into a macropinosome. Finally, we modulate the rate  
72 of macropinocytosis using stimulation and pharmacological inhibition to demonstrate that the ruffle  
73 morphology is unaffected, but PI3K activity is required to prime ruffle membranes for sealing into  
74 macropinosomes.

## 75 **Results**

### 76 **LLSM allows volumetric visualization of plasma membrane movements relative to PIP<sub>3</sub> and PI(3,4)P<sub>2</sub>** 77 **distribution during macropinocytosis**

78 Our first objective was to capture the 3D structure of the plasma membrane relative to the PI3K activity  
79 during macropinosome formation. LLSM imaging was performed on fetal liver macrophages (FLMs) stably  
80 expressing the fluorescent proteins mNeonGreen localized to the plasma membrane via the lipidation  
81 signal sequence from Lck (mNG-Mem) and mScarlet-I fused to the pleckstrin homology domain of Akt  
82 (mSc-AktPH). The AktPH probe recognizes PIP<sub>3</sub> and PI(3,4)P<sub>2</sub> with similar affinity and has been used  
83 extensively to characterize PI3K activity during macropinocytosis<sup>8</sup>. LLSM imaging of mNG-Mem allowed  
84 visualization of plasma membranes via isosurface renderings in the molecular visualization software,  
85 ChimeraX<sup>27</sup>. These images were of sufficient resolution that the detailed structure of ruffles and forming  
86 macropinosomes could be observed in living cells (Fig. 1a), similar to scanning electron microscopy  
87 imaging of bone marrow derived macrophages (Fig. 1b). To visualize the recruitment of mSc-AktPH  
88 relative to the membrane, we used volumetric intensity renderings that maintain the spatial distribution  
89 of the fluorescence probes throughout the cellular volume. As can be seen in the volume renderings, the

90 mNG-Mem probe persisted on newly formed intracellular vesicles derived from the plasma membrane.  
91 Moreover, we observed membrane movements throughout the entire formation and early trafficking of  
92 macropinosomes, as well as the recruitment of mSc-AktPH to forming macropinosomes (Fig. 1c,  
93 Supplementary Movie 1). Orthogonal plane slices (orthoplanes) in xy, yz, and xz (0.1  $\mu\text{m}$  thick) showed  
94 that mSc-AktPH was enriched in ruffles to varying degrees and intensely labeled circular structures found  
95 near the base and sides of ruffles (Fig. 1d, Supplementary Movie 2). Orthoplanes are effective for  
96 examining the 2D relationships between the fluorescent signals, but can also produce incomplete or  
97 distorted perspectives that are resolved by viewing the full volumetric data (Supplementary Figure 1);  
98 such as when a macropinosome appears closed vs open. Additionally, it is difficult to perceive depth in  
99 the still frame volumetric renderings. To overcome this limitation, we implemented a mesh derived from  
100 the mNG-Mem isosurface with transparent faces that enables visualizing the underlying volumetric mSc-  
101 AktPH signals while maintaining the structural framing needed to resolve plasma membrane  
102 rearrangements (Fig. 1e). Together, these visualization techniques were applied to 122 macropinosome  
103 formations and enable correlating the location and timing of PI3K activity to the membrane extension,  
104 curvature, and fusion of macropinosomes with unprecedented spatial and temporal resolution.

#### 105 **mSc-AktPH is recruited early during ruffle expansion and peaks at the base of ruffles after** 106 **macropinosome sealing.**

107 In prior analysis of macropinocytosis using microscopy methods with low axial resolution, AktPH was  
108 recruited as ruffles transitioned into closed circular ruffles and nascent macropinosomes<sup>8</sup>. Here, the  
109 enhanced z-axis resolution and detection sensitivity of LLSM enabled visualizing the dynamic recruitment  
110 of mSc-AktPH to ruffles as they began to protrude from the plasma membrane (Fig. 2a) until maturation  
111 where tubulation and fusion between adjacent macropinosomes occurs (Supplementary Movie 3). As  
112 these early ruffles expanded laterally along the plasma membrane and protruded vertically from the cell  
113 surface, some ruffles continued to accumulate mSc-AktPH, whereas others lost mSc-AktPH and receded  
114 back into the cell suggesting different levels of PI3K activity in neighboring ruffles influences the outcome  
115 of a ruffling region (Fig. 2b). Ruffles that maintained mSc-AktPH throughout the ruffle volume continued  
116 to grow and formed macropinosomes, which were accompanied by an intense transient recruitment of  
117 mSc-AktPH to the base of the ruffle around the nascent macropinosome (Fig. 2c, Supplementary Movie  
118 4). Given the early localization and amplification of PI3K signaling in ruffles that become macropinosomes,  
119 we wondered if PI3K activity contributed to 3D ruffle dynamics.

#### 120 **PI3K activity is required for macropinosome sealing, but not ruffling or closure**

121 To gain insight into the role of PI3K in regulating the morphological dynamics of macropinocytosis, we  
122 used the broad-spectrum PI3K inhibitor LY294002, which inhibits the closure phase of macropinocytosis  
123 in macrophages<sup>24</sup>. Non-treated control cells formed transient dorsal ruffles that recruited mSc-AktPH and  
124 closed into macropinosomes, as seen by the surface rendering and intracellular void that is maintained in  
125 the plane view (Fig. 3a-c, Supplementary Movie 5). LY294002 treatment did not impact ruffle formation,  
126 but eliminated mSc-AktPH recruitment to membrane ruffles (Fig. 3d,e, Supplementary Movie 6).  
127 Furthermore, LY294002-treated cells frequently formed ruffles that appeared to close into a  
128 macropinosome but retracted back to the plasma membrane and failed to maintain an intracellular

129 organelle (Fig. 3f). Taken together, these data suggest that PI3K activity is dispensable for ruffle formation  
130 and membrane collision but is required for membrane sealing to generate a macropinosome.

### 131 **PI3K activity primes ruffles for fusion to seal nascent macropinosomes**

132 We next sought to categorize the macropinosome formation based on the way the membrane fused and  
133 the relative amount of PI3K activity. Based on the previously established models for macropinosome  
134 formation there would be distinguishing characteristics depending on the sealing method. Either we  
135 would find linear extensions where the distal tips would collide to circularize and seal, or there would be  
136 filopodia-like spikes that form, the membrane would fill in the space between before twisting to seal.  
137 Surprisingly, we found that approximately 88% of the quantified macropinosomes formed when the  
138 leading edge of extending ruffles collided along the sides of nearby membrane surface or ruffles that  
139 typically only involved a small portion of the second ruffle, so long as the ruffle area had elevated mSc-  
140 AktPH (Fig. 4). The remaining 12% of events we observed were classified as tidal-wave like structures in  
141 which a mostly isolated planar ruffle extended from the cell surface where the entire ruffle was rich in  
142 mSc-AktPH, the ruffle gained curvature in a rolling fashion, and resulted in fusing with the plasma  
143 membrane (Supplementary Movie 5). However, given that the entire ruffle area was rich in mSc-AktPH,  
144 these types of formation follow the same underlying mechanism as collisions with adjacent membrane  
145 extensions. Frequently, a single ruffle area produced multiple macropinosomes and were the result of  
146 similar but smaller ruffle extensions that quickly fused near the base of larger ruffles (Fig. 4). Within the  
147 ruffle, forming macropinosomes recruited mSc-AktPH near the base of the ruffle as they transitioned into  
148 a spherical shape prior to detaching from the plasma membrane and moving independently (Fig. 4,  
149 Supplementary Movies 3,7). We hypothesized that regions with highly concentrated mSc-AktPH  
150 localization would correlate with increased macropinocytic activity. Indeed, this phenomenon was  
151 observed in four of the eleven constitutive cells (Fig. 5). These ruffling regions resulted in the formation  
152 of many macropinosomes through the intersection of multiple ruffles that were nearly indistinguishable  
153 from one another and only became apparent through the PI3K post closure activity (Fig. 5d,e). Therefore,  
154 the elevated PI3K activity created a microenvironment suited for the rapid fusion of PI3K- primed ruffles  
155 into macropinosomes of various sizes within short timeframes (Supplementary Movies 8,9). We  
156 speculated that other signaling that activates PI3K activity may stimulate distinct ruffling morphologies  
157 and rates of macropinocytosis.

### 158 **CSF-1 growth factor signaling promotes extensive circular ruffling and macropinocytosis**

159 CSF-1 is an essential macrophage growth factor that stimulates macropinocytosis at levels controlled by  
160 the concentration of the CSF-1 signal<sup>9</sup>. Macrophages starved of CSF-1 for 24 hrs and then acutely  
161 stimulated produced expansive circular ruffles that initiated from the distal cellular margins coincident  
162 with cellular spreading (Fig. 6). LLSM imaging revealed a circular ruffle that initiated at the edge of the cell  
163 with a height of approximately 2  $\mu\text{m}$  above the dorsal surface and constricted to a central location in a  
164 coordinated manner (Fig. 6a). A striking feature of this ruffle was the confinement of mSc-AktPH within  
165 the limiting edge of the ruffle. As the circular ruffle constricted toward the center of the cell, mSc-AktPH  
166 was highly concentrated within and was nearly undetectable in the rest of the cell (Fig. 6b, Supplementary  
167 Movie 10), and macropinosomes formed during the constriction process without additional membrane  
168 protrusions being generated. This is consistent with PI3K activity priming membranes for fusion through

169 a purse-string closure to generate macropinosomes (Fig. 6c, Supplementary Movies 10,11). Thus, CSF-1  
170 initiated long range signaling and PI3K activation resulting in coordinated movements of the cytoskeleton  
171 throughout the cell.

## 172 **LPS stimulates regional ruffling and generates large numbers of macropinosomes**

173 The bacterial cell wall component lipopolysaccharide (LPS) activates PI3K through the Akt pathway<sup>28</sup>, and  
174 acutely stimulates macropinocytosis<sup>3</sup>. Recently, LPS stimulation was used to characterize a novel  
175 formation mechanism involving actin tentpoles supporting membrane veils which cross to create a  
176 macropinosome<sup>12</sup>. When FLMs were exposed to LPS, regional patches of membrane ruffling were  
177 generated that migrated around the dorsal surface of the macrophage (Fig. 7a, Supplementary Movie 12)  
178 in a manner distinct from the dorsal surface ruffle generated by CSF-1 stimulated cells (Fig. 6); however,  
179 this process was similar in appearance to constitutive macropinocytosis (Fig. 7c, Supplementary Movie  
180 13). The patches of ruffles in LPS cells generated many small ruffles, had elevated PI3K activity and were  
181 more efficient at forming macropinosomes as compared to control (Fig 7d). Thus, the nature of  
182 macropinosome formation is coordinated over different length scales with differing intensities depending  
183 on the nature of the activating stimulus. Regardless, PI3K activity delineates ruffles and regions of the  
184 plasma membrane where macropinosomes form.

## 185 **Discussion & Conclusion**

186 Here, we have utilized lattice light sheet microscopy to develop a new level understanding of the  
187 structural dynamics and PI3K signaling underpinning macropinocytosis. Until recently, dynamic processes  
188 such as macropinocytosis were characterized using optical techniques with poor axial resolution and  
189 elevated phototoxicity leading to subsampling the spatial and temporal dynamics and requiring inference  
190 from multiple methods such as scanning electron microscopy of fixed cells to address the formation  
191 mechanism of macropinosomes. Lightsheet microscopy overcomes these obstacles and enables us to  
192 record, with sufficient spatial and temporal resolution, the complete evolution of membrane ruffles and  
193 the mechanism by which these ruffles form into macropinosomes, while also measuring the redistribution  
194 of signaling molecules controlling these processes. We have shown that macropinosomes form through  
195 several possible morphologies; however, in each case PI3K activity primes ruffles for fusion with adjacent  
196 primed membranes to form macropinosomes. Indeed, in areas with elevated PI3K activity, either naturally  
197 or through external stimulation, there was an increased ruffle density that lead to an increased probability  
198 of primed ruffles colliding to form macropinosomes. This model of macropinosome formation relying on  
199 PI3K priming rather than a defined geometry also explains the variation in diameter that is a hallmark of  
200 macropinosomes. The improved sensitivity of LLSM enabled detection of PI3K activity at the earliest  
201 stages of ruffle development that grows in curving ruffles and peaks around macropinosomes post  
202 closure. Our data are consistent with a mechanism driven by the geometry of curving ruffles that confines  
203 PI3K, thereby amplifying the signal, which in turn activates yet unknown fusogenic protein(s) localized to  
204 the ruffle edges mediating sealing during membrane collisions. This conclusion is supported by the  
205 observations that inhibition of PI3K activity with LY29004 did not substantially alter membrane ruffling  
206 structure, curvature or collisions, but completely inhibited sealing; even when fully spherical  
207 morphologies were observed that then collapsed back into the cell surface.

208 The model suggested in this work contrasts with a recent report in LPS-activated RAW264.7 cells that  
209 described F-actin-rich filopodia-like “tentpoles” protruding from the surface that twisted to constrict veils  
210 of membrane that then became macropinosomes<sup>12</sup>. Using a membrane probe and the same microscope,  
211 we should have recapitulated the filopodial-like protrusions in the initial extension-phase that then would  
212 have a concave appearance connecting the tips. Only rarely when visualizing single slices of ruffling  
213 membrane, did we observe filopodial-like extensions connecting at the distal margins (Supplementary  
214 Figure 1b). However, the isosurface and volumetric renderings of the same macropinosocytic events were  
215 not filopodial-like but were, in fact, multiple linear ruffle sheets that protruded from the cell surface and  
216 intersected to form a macropinosome (Supplementary Figure 1c). Additionally, these ruffles protruding  
217 from the cell were convex as they emerged and formed which fits a model where actin polymerization  
218 occurs throughout the ruffle driving the extension forward.

219 Taken together, our experiments indicate a mechanism for macropinosome formation requiring amplified  
220 PI3K signaling within ruffles that become macropinosomes and contributes primarily to priming  
221 membranes for sealing. The membrane probe and visualizations we have described set the foundation to  
222 enable rigorous testing of this mechanism using specific inhibitors of phosphatidylinositol-modifying  
223 enzymes and sensors that specifically bind to the various products to determine how each step is  
224 regulated during macropinocytosis.

## 225 **Methods and Materials**

226 **Plasmids.** pCMV-VSV-G was a gift from Bob Weinberg (Addgene plasmid #8454;  
227 <http://n2t.net/addgene:8454>; RRID:Addgene\_8454)<sup>29</sup>. psPAX2 was a gift from Didier Trono (Addgene  
228 plasmid #12260; <http://n2t.net/addgene:12260>; RRID:Addgene\_12260). pLJM1-EGFP was a gift from  
229 David Sabatini (Addgene plasmid #19319 ; <http://n2t.net/addgene:19319> ; RRID:Addgene\_19319)<sup>30</sup>. Lck-  
230 mScarlet-I was a gift from Dorus Gadella (Addgene plasmid #98821; <http://n2t.net/addgene:98821>;  
231 RRID:Addgene\_98821)<sup>31</sup>.

232 **Construction of the membrane and AktPH probes.** The membrane probe was constructed by combining  
233 the membrane localization motif (MGCVCSSNPE) from Lck<sup>31</sup> in frame with mNeonGreen in the pLJM1  
234 backbone containing the puromycin resistance gene. The mSc-AktPH probe was constructed by using  
235 mScarlet-I in frame with the pleckstrin homology domain from Akt in the pLJM1 backbone, modified to  
236 contain the blasticidin resistance gene. Sequences were codon optimized for expression in mouse cells,  
237 synthesized, and sequence verified by GenScript (Piscataway, NJ).

238 **Viral transduction.** Sequence-verified plasmids containing genes encoding FP-chimeras, plus the  
239 packaging plasmids pVSV-G and psPAX2 were transfected into NIH 293T cells for packaging using linear  
240 25 kDa polyethylenimine (PEI) as a transfection reagent. NIH 293T-cell culture supernatant containing  
241 lentiviral particles was collected and added to FLM treated with cyclosporin A (10  $\mu$ M) for two days.  
242 Transduced FLMs were selected with puromycin and blasticidin (10  $\mu$ g·ml<sup>-1</sup> each).

243 **Macrophage culture media.** DMEM/F-12 (Gibco) supplemented with 20% Heat-inactivated FBS (R&D  
244 Systems), 1% Penicillin/Streptomycin (Gibco), 50 ng·ml<sup>-1</sup> mCSF-1 (BioLegend), and 5  $\mu$ g·ml<sup>-1</sup> plasmocin  
245 (Invivogen) maintained at 37°C with 7.5% CO<sub>2</sub>.

246 **PIP<sub>3</sub> inhibition (LY294002).** Coverslips were prepared as described previously and were moved to a well  
247 of media containing 0.16  $\mu\text{M}$  LY294002 and allowed to incubate for 30 minutes at 37°C and 7.5% CO<sub>2</sub> prior  
248 to imaging. The coverslip was then transferred to the LLSM bath containing Imaging Media, 1.7 mM  
249 Glucose, and 0.16  $\mu\text{M}$  LY294002. The coverslip was explored using the LLS software and three cells were  
250 chosen per coverslip that provided the best visual representation of the population. Each cell was imaged  
251 under the same parameters as described above.

252 **CSF-1 stimulation.** The coverslip was starved overnight in DMEM/F-12 with 10% FBS and 1% pen/strep.  
253 After 24hrs the coverslip was moved to the LLS bath containing 7mL L-15 imaging media, and 1.7mM  
254 Glucose. The coverslip was explored using the LLS software and three cell targets were chosen and imaged  
255 for a pre-stimulation comparison. Immediately after imaging the third cell, CSF-1 was introduced at 50 ng  
256  $\cdot\text{mL}^{-1}$  to the 7 mL bath. The third cell was once again imaged <1min after stimulation and each additional  
257 cell was imaged in reverse order (Imaging order 1-2-3-3-2-1).

258 **Lipopolysaccharide stimulation.** FLMs were stimulated with 100 ng $\cdot\text{ml}^{-1}$  Lipopolysaccharides from  
259 *Salmonella enterica* serotype enteritidis (Sigma) for 24 h in culture media before being transferred to  
260 imaging media containing 100 ng $\cdot\text{ml}^{-1}$  for LLSM experiments.

261 **Macrophage isolation.** Fetal liver macrophage (FLM) cell cultures were generated as described  
262 previously<sup>32,33</sup>. Livers were isolated from gestational day 15-19 mouse fetuses from C57BL/6J mice (The  
263 Jackson Laboratory, Bar Harbor, ME) in accordance with South Dakota State University Institutional  
264 Animal Use and Care Committee. Liver tissue was mechanically dissociated using sterile fine-pointed  
265 forceps and a single-cell suspension was created by passing the tissue through a 1 ml pipette tip<sup>32</sup>. Cells  
266 were plated on non-tissue culture treated dishes and kept in growth and differentiation medium  
267 containing the following: 20% heat-inactivated fetal bovine serum; 30% L-cell supernatant, a source of M-  
268 CSF<sup>34,35</sup>; and 50% Dulbecco's modified growth medium containing 4.5 g $\cdot\text{L}^{-1}$  glucose, 110 mg  $\text{L}^{-1}$  sodium  
269 pyruvate, 584 mg $\cdot\text{L}^{-1}$  L-glutamine, 1 IU  $\text{ml}^{-1}$  penicillin and 100  $\mu\text{g}\cdot\text{ml}^{-1}$  streptomycin. FLM were cultured for  
270 at least 8 weeks prior to transduction and experiments.

271 **Cell Culturing and Coverslip Plating.** FLMs were cultured in untreated T-25 tissue culture flasks using the  
272 following culture media: DMEM F-12 with 20% FBS, 1% penicillin/streptomycin, 50 ng $\cdot\text{ml}^{-1}$  CSF-1, and 5  
273 ng $\cdot\text{ml}^{-1}$  plasmocin. The cell cultures were split at ~85% confluence, first by washing the T-25 flask with 3  
274 mL of PBS (-Ca/-Mg) 2 times. The cells were then lifted from the T-25 flask using 4 mL of 4°C PBS (-Ca/-  
275 Mg, +0.98mM EDTA) with gentle pipet washing for approximately 10 min. The lifted cells were moved to  
276 a 15 mL centrifuge tube (1 mL of culturing media was added to 15 mL tube if cells took >10 min to lift) and  
277 centrifuged at 200 x g for 5min. While the cells were being spun down, the T-25 flask was washed with  
278 PBS (-Ca/-Mg), filled with 5mL of culture media, and placed in the 37°C incubator to reach appropriate  
279 culture conditions. Once the cells were finished being spun down, the supernatant was removed from the  
280 15 mL tube and the cells were resuspended in 1 mL culturing media and counted. The counting was done  
281 by mixing 10  $\mu\text{L}$  of suspended cells with 10  $\mu\text{L}$  of trypan blue and placed on a glass slip to be counted using  
282 a countess. The FLMs were re-plated in the original T-25 flask with  $\sim 6\text{-}7 \times 10^5$  cells. The cells were washed

283 every 2 days and given fresh media until reaching ~85% confluence where they would then be split. Cell  
284 lines were kept for approximately 2 months before being replaced with early state frozen aliquots.  
285 Macrophages were prepared for LLS imaging 24 h prior to imaging using 5mm glass coverslips. The  
286 coverslips were soaked in 90-100% ethanol and flame cleaned using a butane flame. Approximately 5  
287 flame cleaned coverslips were placed per well of a 12 well plate each containing 1 mL of culture media.  
288 Cells were added to each well during the cell culture process described above at  $\sim 3 \times 10^5$  cells to each  
289  $3.5 \text{ cm}^2$  (12-well plate) for imaging. The FLMs incubated on the flame cleaned glass coverslips in culturing  
290 media for 24 h prior to imaging. The coverslips were transferred to the LLSM bath that was filled with 7  
291 mL of Leibovitz's L-15 Media (supplemented with 1.7 mM glucose) at  $\sim 37^\circ\text{C}$ .

292 **Lattice Light Sheet Microscopy Imaging.** The LLSM is a replica of the design described by Chen et al.<sup>36</sup>,  
293 built under license from HHMI. Volumetric image stacks were generated using dithered square virtual  
294 lattices (Outer NA 0.55, Inner NA 0.50, approximately 30  $\mu\text{m}$  long) and stage scanning with 0.5  $\mu\text{m}$  step  
295 sizes, resulting in 254 nm deskewed z-steps. Excitation laser powers used were  $18 \mu\text{W}$  (488 nm) and  $22 \mu\text{W}$   
296 (561 nm), measured at the back aperture of the excitation objective. The emission filter cube (DFM1,  
297 Thorlabs) comprised a quadband notch filter NF03-405/488/561/635 (Semrock), longpass dichroic mirror  
298 Di02-R561 (Semrock), shortpass filter 550SP (Omega) on the reflected path, and longpass filter BLP01-  
299 561R (Semrock) on the transmitted path; the resulting fluorescence was imaged onto a pair of ORCA-  
300 Flash4.0 v2 sCMOS cameras (Hamamatsu). The camera on the reflected image path was mounted on a  
301 manual x-y-z translation stage (Newport 462-XYZ stage, Thorlabs), and the images were registered using  
302 0.1  $\mu\text{m}$  Fluoresbrite YG microspheres (Polysciences). The image capturing rates varied between 5-10  
303 seconds per volume using 8-12 ms planar exposures depending on the brightness of the cell and imaging  
304 region.

305 **Scanning Electron Microscopy.** BMDM were plated onto 13 mm diameter, circular glass coverslips and  
306 cultured overnight in RPMI with 10% FBS (R10). To stimulate macropinocytosis, BMDM were incubated  
307 30 min in phosphate-buffered saline (PBS), then 15 min in PBS containing 10 nM CSF-1. Cells were fixed in  
308 2% glutaraldehyde, 0.1 M cacodylate buffer, pH 7.4, 6.8% sucrose, 60 min at  $37^\circ\text{C}$ . Fixative was replaced  
309 with a second fixative consisting of 1%  $\text{OsO}_4$  in 0.1 M cacodylate buffer, pH 7.4, for 60 min at  $23^\circ\text{C}$ . The  
310 second fixative was replaced with 1% tannic acid in cacodylate buffer, 30 min at  $4^\circ\text{C}$ , the rinsed with 3  
311 changes of 0.1 M cacodylate buffer. Coverslips were transferred through successive changes of acetone-  
312 water mixtures, progressively increasing acetone concentrations to 100% before a final incubation in  
313 hydroxymethylsilazidane (HMDS, EM Sciences). HMDS was removed and coverslips were dried for 2 days.  
314 Coverslips were shadowed with gold and observed on a Amray 1900 field emission scanning electron  
315 microscope.

316 **Deconvolution and Post Processing.** The raw volumes acquired from the LLSM were deskewed,  
317 deconvolved and rotated to coverslip coordinates in LLSpy<sup>37</sup>. We applied a fixed background subtraction  
318 based on an average dark current image, 10 iterations of Lucy-Richardson deconvolution with  
319 experimentally measured point spread functions for each excitation followed by rotation to coverslip  
320 coordinates, and cropping to the region of interest surrounding the volume for visualization. We  
321 optimized the illumination intensity such that less than 10% photobleaching occurred during the  
322 experiment. The fully processed data was opened as a volume map series in UCSF ChimeraX and utilized  
323 isosurface, mesh, 3D volumetric intensities, and orthogonal planes renderings to exam the data. The

324 surface and mesh options utilize a three-dimensional analog of an isoline called an isosurface that  
325 represents points in volume space as constant values which were used to display the membrane probe.  
326 The isosurface provides a defined surface for the membrane probe resulting in shadowing providing visual  
327 depth to the three-dimensional data. The mesh rendering offers a similar surface definition while also  
328 providing an option to include the internal fluorescent mSc-AktPH signal. We used a volumetric intensity  
329 projection to visually display the localization of mSc-AktPH throughout the cell. At each pixel, the most  
330 intense color value underlying the pixel along the line of sight is displayed (ChimeraX User Guide). The  
331 final technique used to display the LLSM data was through orthogonal planes. This generates 2D planes  
332 each 0.128  $\mu\text{m}$  thick for the entire volume in xy, yz, and xz. Multiple methods were overlapped and shown  
333 side by side to effectively represent the data and labeled within each figure.

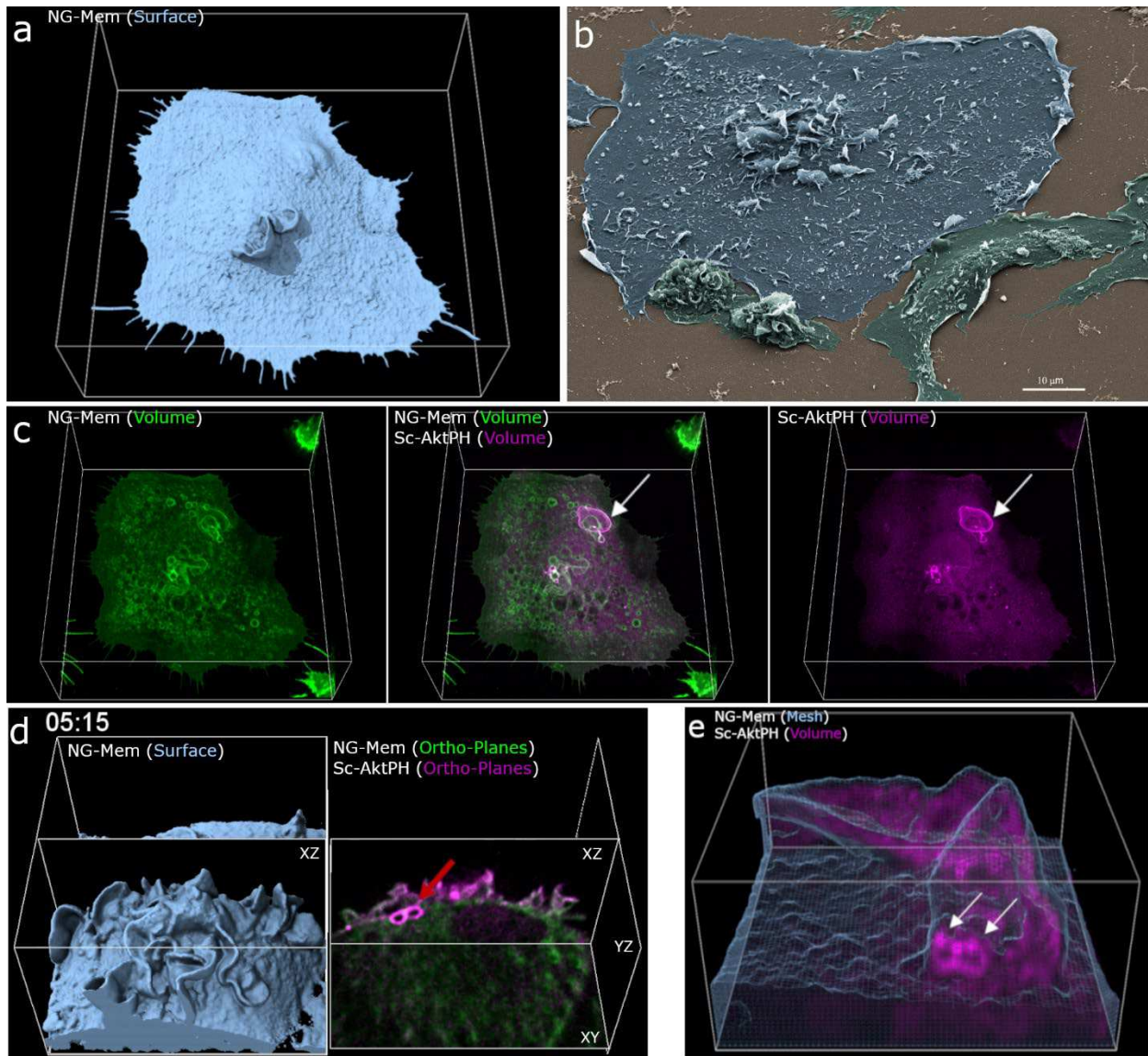
### 334 **Acknowledgments**

335 *Funding:* Funding provided by the South Dakota Board of Regents through BioSNTR and the SDBOR FY20  
336 collaborative research award "IMAGEN: Biomaterials in South Dakota". Additional funding provided by the National  
337 Science Foundation through research award CNS-1626579 "MRI: Development of a Scalable High-Performance  
338 Computing System in Support of the Lattice Light-sheet Microscope for Real-time Three-dimensional Imaging of  
339 Living Cells". J.A.S. was supported by NIH grant R35 GM131720. B.L.S. is supported by the Chan Zuckerberg Initiative  
340 through the Imaging Scientist program.

341 *Visualization:* The data visualization and analyses were performed using UCSF ChimeraX, developed by the  
342 Resource for Biocomputing, Visualization, and Informatics at the University of California, San Francisco, with support  
343 from National Institutes of Health R01-GM129325 and the Office of Cyber Infrastructure and Computational Biology,  
344 National Institute of Allergy and Infectious Diseases.

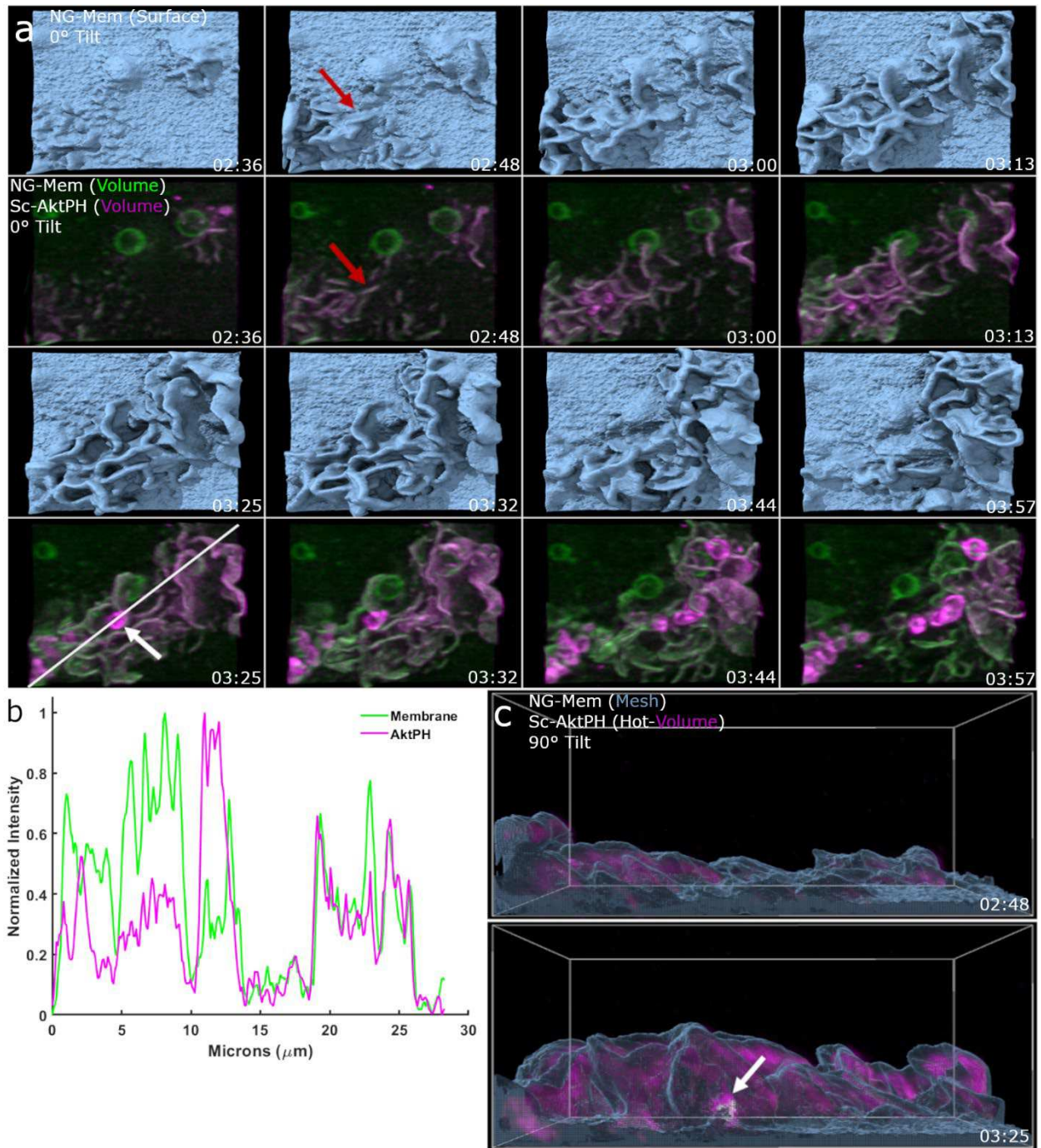
345 *LLSM:* The Lattice Light Sheet Microscope referenced in this research was developed under license from Howard  
346 Hughes Medical Institute, Janelia Farms Research Campus ("Bessel Beam" patent applications 13/160,492 and  
347 13/844,405).

348 *Author Contributions:* S.E.Q. acquired and analyzed LLSM data and co-wrote the manuscript. L.H generated FLM cell  
349 lines used in experiments. J.G.K. Designed plasmid constructs and generated FLM cell lines. J.A.S. Performed SEM  
350 experiments and edited the manuscript. S.S. provided supervision and edited the manuscript. A.D.H. co-wrote the  
351 manuscript. R.B.A. built the LLSM and analysis cluster and provided supervision. N.W.T. designed experiments and  
352 co-wrote the manuscript. B.L.S. designed and performed initial experiments, assisted with data analysis and co-  
353 wrote the manuscript.

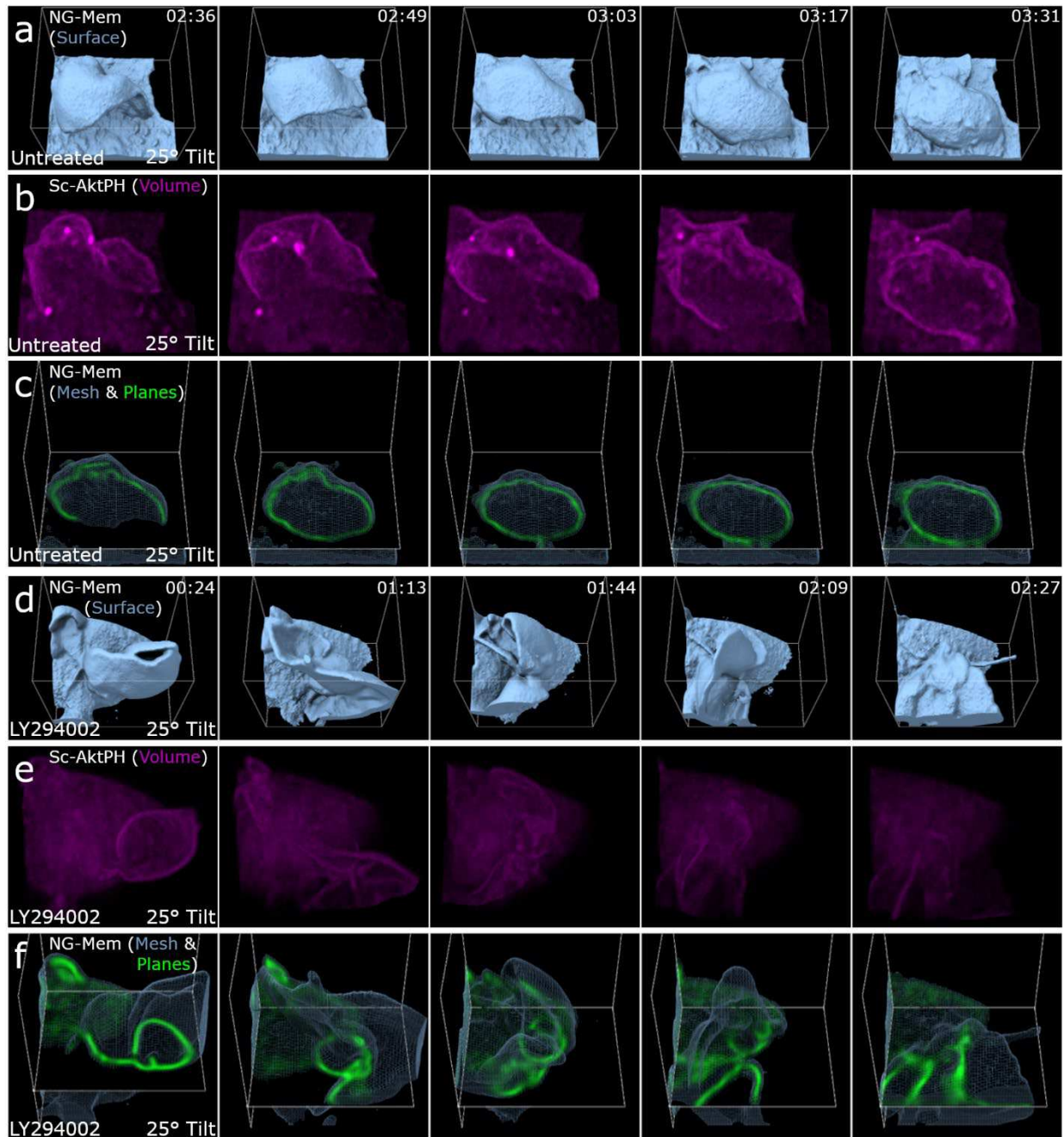


354  
 355  
 356  
 357  
 358  
 359  
 360  
 361  
 362  
 363  
 364  
 365

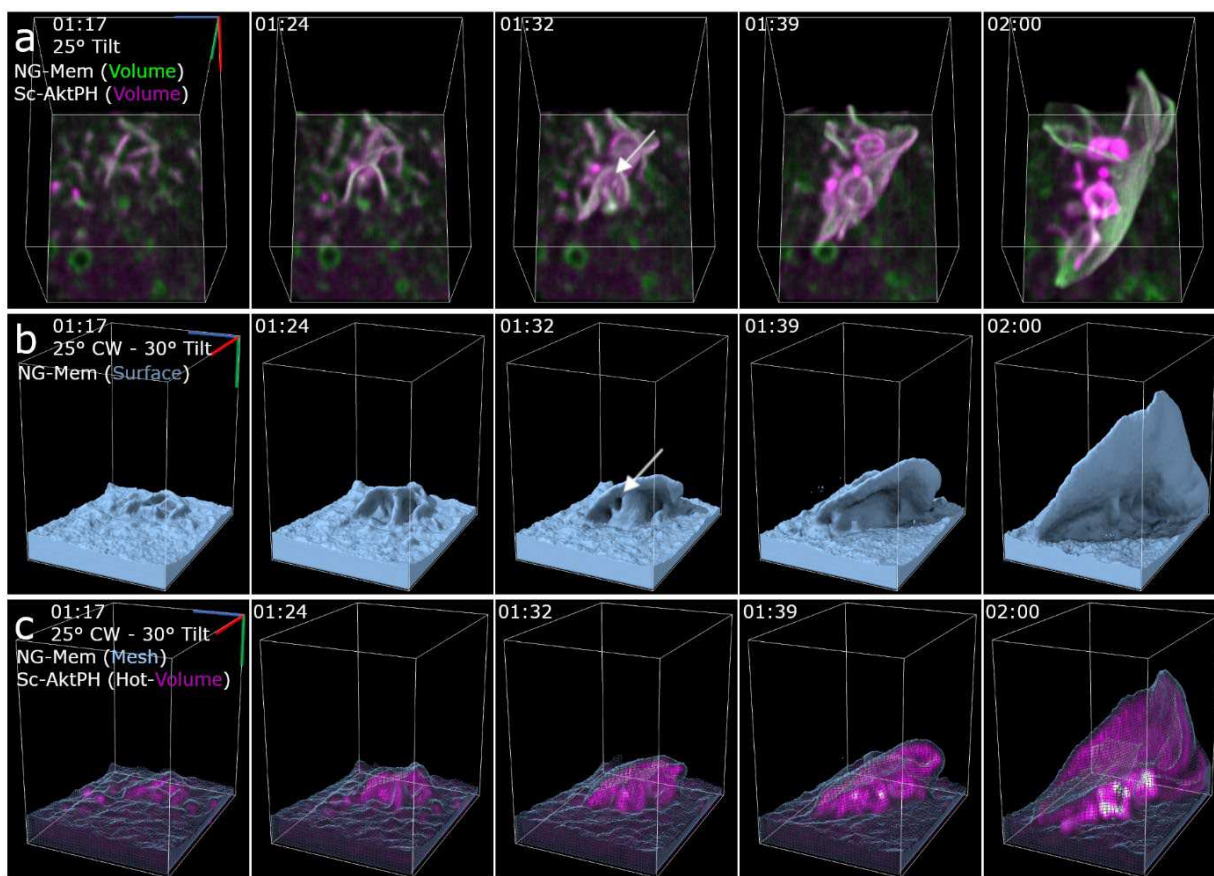
**Figure 1. 3D visualization of macrophages allows insight into membrane structure and phosphatidylinositol dynamics during macropinocytosis.** a) Isosurfaces show the plasma membrane of a live cell that is actively macropinocytosing. Region 68x72x25  $\mu\text{m}$  (x, y, z). b) SEM image of a macrophage acutely stimulated with CSF-1 shows high-resolution fixed cells. Scale bar is 10  $\mu\text{m}$ . c) Volumetric intensities show specific local fluorescence (left-to-right) volumetric membrane (green), dual volumetric membrane and mSc-AktPH (magenta). Volumetric renderings provide a method to visualize the transient fluorescent intensities throughout the volume of the cell. Region is 68x72x25  $\mu\text{m}$ . d) Combinations of visualization techniques such as Isosurface (left) displayed alongside orthogonal planes (right) further clarify how each plane is chosen to show internal intensities. Region of 29x30x19  $\mu\text{m}$ . e) Mesh rendering of the mNG-membrane probe along with volumetric mSc-AktPH provides a representation of the plasma membrane structure as well as underlying fluorescence. The white arrows indicate the post closure recruitment of mSc-AktPH. Region 13x14x7  $\mu\text{m}$ . Different rendering methods provide insight into cellular characteristics such as structure, depth, and fluorescent intensity and provide a foundation for visualizing localization of mSc-AktPH to the constantly changing plasma membrane during macropinocytosis.



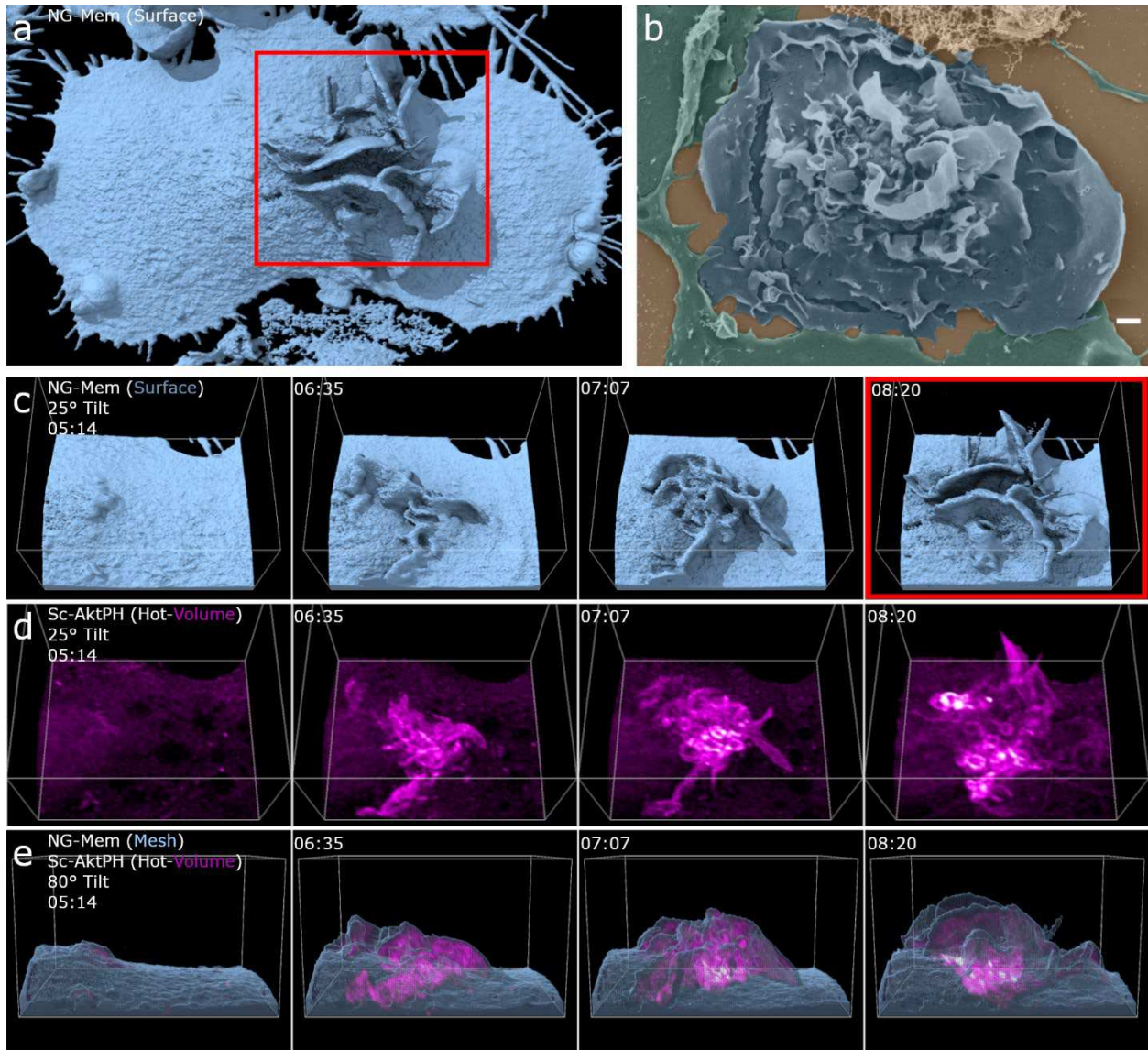
366  
 367 **Figure 2. Early PI3K activity leads to amplification of PIP<sub>3</sub>/PIP<sub>2</sub> in developing ruffles, macropinosome formation, and post closure recruitment.**  
 368 a) Top view of an mNG-mem isosurface rendering provides depth for 3D visualization of ruffle extension. Dual-color volumetric intensity display  
 369 comparing the recruitment of mSc-AktPH to early and expanding ruffles as well as sealed macropinosomes (Region 21x19um). b) Intensity line-  
 370 scan of the volumetric mNG-Mem and mSc-AktPH shows their relative intensities for extending membrane ruffles, as well as recruitment around  
 371 a sealed macropinosome. c) Side view of the isosurface mesh plasma membrane and volumetric mSc-AktPH (Magenta Hot color scale) from a  
 372 shows that the early stages of ruffle development is filled with mSc-AktPH and the resulting macropinosome (white arrow) receives a final intense  
 373 mSc-AktPH recruitment around the formed macropinosome at the bottom of the ruffle. Region of 21x19x15um.  
 374



375  
 376  
 377 **Figure 3. PI3K activity is required for membrane sealing and separation from PM/internalization of a complete macropinosome but not**  
 378 **membrane ruffling** a) Isosurface rendering of mNG-mem for an untreated macrophage during a successful macropinosome event where the  
 379 sheet curls back toward the membrane for fusion/sealing. Region 12x13x10  $\mu\text{m}$  b) Volumetric rendering of Sc-AktPH of the untreated cell shows  
 380 the increase of PI3K activity in the ruffle that creates a macropinosome. 12x13x10  $\mu\text{m}$  c) Mesh and orthogonal planes of mNG-mem show the  
 381 internal membrane organization of the ruffle and resulting macropinosome. 12x13x10  $\mu\text{m}$  d) Isosurface rendering of an LY294002 treated  
 382 macrophage provides depth to the attempted closure of a macropinosome. Region 10x12x10  $\mu\text{m}$ . e) Volumetric intensity rendering of Sc-  
 383 AktPH for an LY294002-treated macrophage shows the diffuse distribution of AktPH and minimal PI3K activity. The cytosolic intensities were co-  
 384 scaled for the untreated and treated macrophage. Region 10x12x10  $\mu\text{m}$  f) XY-plane for the mNG-mem probe of an LY294002-treated cell during  
 385 a failed macropinosome event. In the surface view, the ruffle appeared to form a macropinosome; however, when overlaid with the plane view  
 386 it became clear that it failed to fully form into a macropinosome. The ruffle quickly reduced in size and became undistinguishable within the  
 387 cytosol, while never receiving the post closure increase of PI3K activity. Region 10x12x10  $\mu\text{m}$ .  
 388

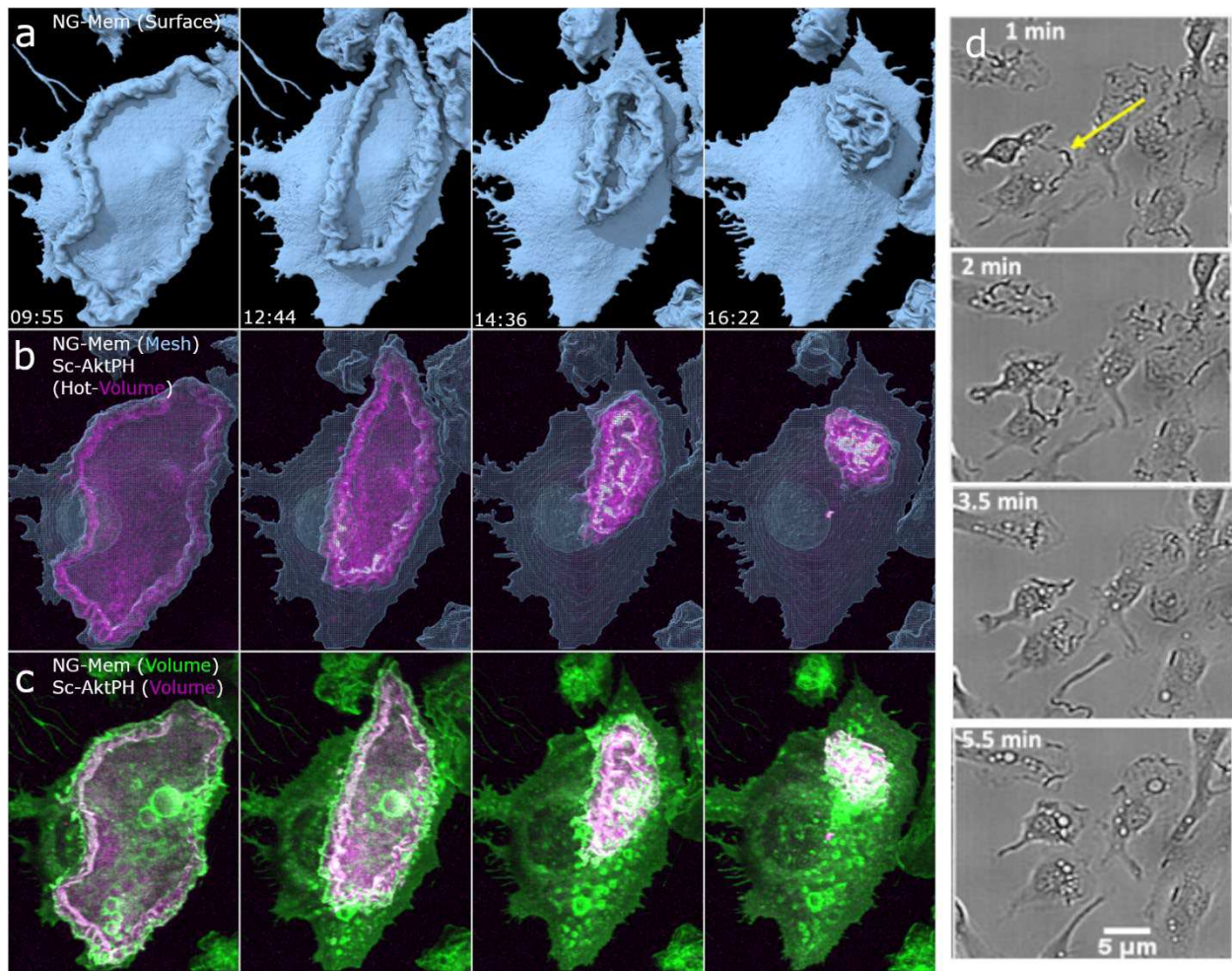


389  
 390 **Figure 4. Macropinosomes form via PI3K-primed ruffle fusion.** a) Dual volumetric intensities of mNG-mem and mSc-AktPH show the intensity  
 391 of each probe as the ruffles and macropinosomes form. The montage shows the earliest stage of the ruffle that extends vertically and forms  
 392 macropinosomes along the length near the base of the primary ruffle as a result of smaller mSc-AktPH-rich extensions colliding. The white arrow  
 393 points at the macropinosome forming region further emphasized in the isosurface. Region 9x12x13  $\mu\text{m}$ . b) Isosurface rendering of mNG-  
 394 membrane shows the structure of the extending ruffle and the continued sheet extension after the macropinosomes formed. The white arrow  
 395 emphasizes the small pocket that closes to form one of the macropinosomes. Region 9x12x13  $\mu\text{m}$ . c) Mesh surface rendering of mNG-mem and  
 396 volumetric mSc-AktPH shows the internalized macropinosome with the increased localization of mSc-AktPH at the bottom of the ruffle. Region  
 397 11x9x12  $\mu\text{m}$ .  
 398



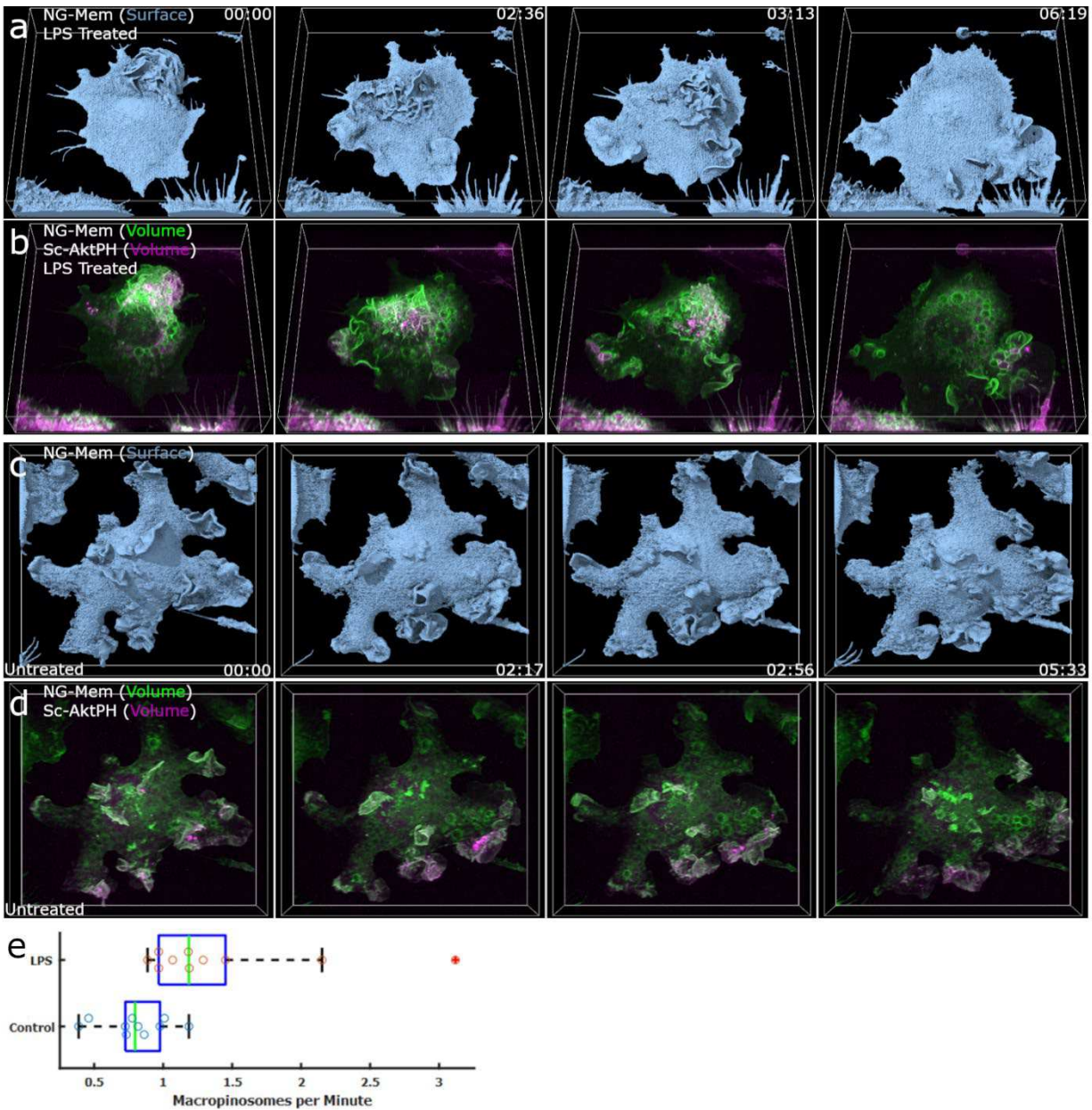
399  
 400  
 401  
 402  
 403  
 404  
 405  
 406

**Figure 5. Phosphatidylinositol localization and chaotic ruffling underlie macropinocytosis in complex membrane structures.** a) Single time point, full cell surface rendering of chaotic macropinocytosis event. The red box correlates to the same frame in c-d. b) SEM images of a BMDM showing similar highly active ruffling regions c) Isosurface montage shows the chaotic orientation of membrane structure. Region 27x22x16  $\mu\text{m}$ , 25° tilt. d) Volumetric AktPH (Magenta-Hot) provides a more detailed emphasis on the AktPH activity within the membrane ruffles and highlights the macropinosomes that have formed. Region 27x22x16  $\mu\text{m}$  with a 25° tilted view. e) Mesh Surface with AktPH (Magenta Hot) shows the AktPH activity as the ruffle develops as well as the increased recruitment around formed macropinosomes at the base of the event.



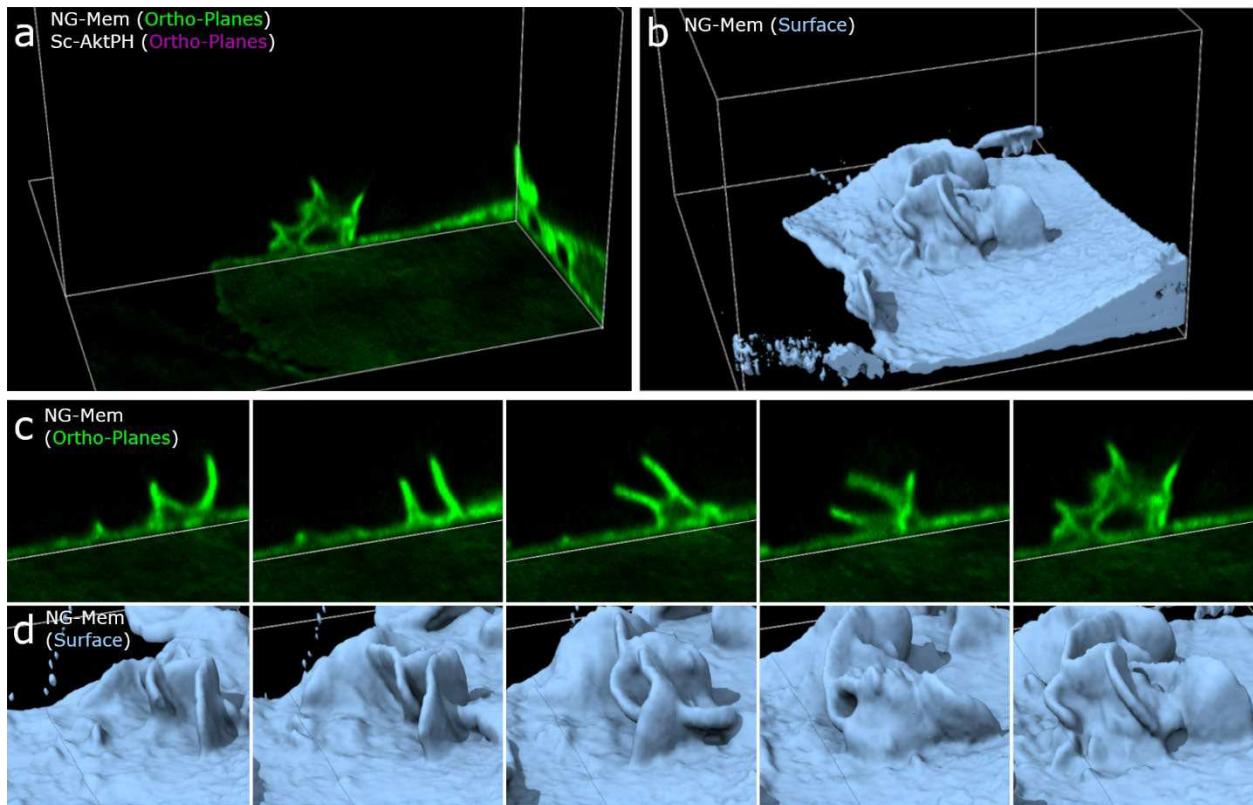
407  
 408  
 409  
 410  
 411  
 412  
 413  
 414  
 415  
 416

**Figure 6. Growth factor starvation and stimulation results in the formation of large circular dorsal ruffles that corral  $PIP_3/PIP_2$ .** Macrophages were starved of CSF-1 for 24 h, imaged for 5 minutes as a baseline, and imaging restarted 1 min after stimulation with  $50 \text{ ng}\cdot\text{mL}^{-1}$  CSF-1. Four-frame montages provide a visual display of the large dorsal ruffle that acts as a diffusional barrier that restricts  $PIP_3/PIP_2$  to the inside of the ruffle as it is cleared from the surface. This barrier is likely acting as a signal amplification mechanism stimulating the production of many macropinosomes. a) Isosurface rendering provides crisp surface directionality, b) Surface mesh and volumetric AktPH (magenta-hot), show the restricted probe as the membrane converges c) Volumetric Intensity of both mNG-Membrane and mSc-AktPH show the intensity locations of the membrane ruffle and the restricted AktPH.  $49\times 60 \mu\text{m}$  d) Bright field images showing multiple cells responding to stimulation with similar dorsal membrane clearing.



417  
418  
419  
420  
421  
422  
423  
424  
425  
426

**Figure 7. LPS stimulation increases membrane ruffling and macropinocytosis.** Macrophages were pretreated with  $100 \text{ ng}\cdot\text{ml}^{-1}$  LPS for 24 h prior to imaging. a) Surface rendering of mNG-Mem on an LPS stimulated macrophage provides a surface level understanding of the membrane, exploration, ruffling, and PM structure. b) Dual-color volumetric intensity projections of mNG-Mem and mSc-AktPH for an LPS stimulated cell provided the intensity activity during increased macrophage activity and shows the highly AktPH rich regions of membrane ruffling. Region  $68 \times 77 \times 21 \mu\text{m}$  c) Untreated macrophage Isosurface showing visibly less exploratory behavior. d) Dual-color volumetric intensity rendering of the untreated macrophage gives insight on the AktPH activity inside of the cell during macropinocytosis and allows for the quantitative comparison of macropinosomes formed between the stimulated and unstimulated cells. Region  $68 \times 77 \times 21 \mu\text{m}$ . e) Box plot showing the difference in macropinosome activity between untreated and LPS treated macrophages. All macropinosomes greater than  $1 \mu\text{m}$  were manually counted using a z-projection MIP in Fiji and were distinguished by the post closure spike in mSc-AktPH intensity.



427  
428 **Supplementary Figure 1 - Constitutive macropinocytosis and the importance of reducing the dimensionality of data.** a) Orthoplane (left) and  
429 isosurface (right) views of mNG-Membrane show the subsurface macropinosome and the complex structure of the full surface. b) Orthoplane  
430 montage of mNG-membrane depicting constitutive planar view of macropinocytosis where two sheets extend from the cell membrane,  
431 circularize, and connect to form a macropinosome. c) Isosurface view of mNG-Membrane showing the three spatial dimensions of the ruffle  
432 clearly depicting the multiple membrane sheets involved in the macropinocytotic event. The red box shows the corresponding montage frames for  
433 panel a.  
434  
435

## 436 Supplementary Movie Legends

437 **Video 1. Corresponds to Fig. 1a, c.** Isosurface and volumetric intensity renderings (Green mNG-Mem; Magenta mSc-AktPH) provides different  
438 methods of visualizing the formation (surface) and trafficking of macropinosomes and mSc-AktPH accumulation (volume). Movie timestamps  
439 highlight the following events: AktPH enriched ruffle development (02:42), newly formed macropinosomes (06:29; 08:51; 10:58), and post closure  
440 AktPH recruitment (11:19). Frame rate of ~7s and each region is 68x72x25  $\mu\text{m}$ .

441 **Video 2. Corresponds to Fig. 1d.** Isosurface rendering in conjunction with orthogonal plans moved through a volume provide ~0.1  $\mu\text{m}$  thick planes  
442 to help visualize the internal and surface activity of mNG-mem and mSc-AktPH including macropinosome closures (02:41; 05:15), membrane rich  
443 ruffles (00:00; 02:34; 05:08), previously formed internal macropinosomes (05:15 during scan), and mSc-Akt localization around a closed  
444 macropinosome (05:15 during scan). Framerate of ~7s and two subregions each 29x30x19  $\mu\text{m}$ .

445 **Video 3. Corresponds to Fig. 2a.** Isosurface and dual-volumetric intensity projection of mNG-mem and mSc-AktPH with a 25 degree tilt shows a  
446 variety of formation events. Several early formations occur prior to relaxation of the plasma membrane (01:58), followed by the development of  
447 another AktPH rich ruffle (02:48), membrane closure into a macropinosome (03:07 -> 3:13), and finally post closure recruitment of AktPH (03:25).  
448 Several macropinosomes form that are indicated by the recruitment of AktPH post closure (3:57; 07:16) and subsequently trafficked toward one  
449 another to merge (4:53; 05:18; 05:30; 07:54). Frame rate of ~6.25s and region of 21x19x15  $\mu\text{m}$ .

450 **Video 4. Corresponds to Fig. 2c.** Mesh rendering of mNG-membrane and volumetric intensity projection of mSc-AktPH (Magenta-Hot) using a 90  
451 degree tilt. The second play through contains a pause to emphasize the frame shown in Fig 2c and highlight the AktPH rich membrane ruffles  
452 (02:48) and the post closure recruitments (03:25; 03:57). Frame rate ~6.25s region of 21x19x15  $\mu\text{m}$ .

453 **Video 5. Corresponds to Fig. 3a, b.** Isosurface in conjunction with three volumetric intensity renderings (Green mNG-Mem; Magenta mSc-AktPH)  
454 display a traditional formation in an untreated cell including the initial ruffle (00:00) that vertically extends and begins to form a tidal wave (01:31)  
455 back toward the surface of the cell, with membrane scission (03:24 -> 03:31) and finally the post closure recruitment for the largest  
456 macropinosome (08:07). Frame rate of 7s and Region of 12x13x10  $\mu\text{m}$

457 **Video 6. Corresponds to Fig. 3d, e.** Isosurface with three volumetric intensity renderings (Green mNG-Mem; Magenta mSc-AktPH) on an LY294002  
458 treated macrophage showing the initial ruffle with uniform AktPH throughout the cytosol and ruffle (00:00), attempted closure of the ruffle  
459 (00:30), continued compression of the attempted macropinosome (00:30 -> 02:27), becoming un-trackable within the cytosol with no AktPH  
460 recruitment to the attempted macropinosome. (Tracking done manually using orthogonal planes) Frame rate of 6.15s and Region 10x12x10  $\mu\text{m}$ .

461 **Video 7. Corresponds to Fig. 4a, b.** Isosurface alongside three volumetric intensity renderings (Green mNG-Mem; Magenta mSc-AktPH) shows  
462 the formation of macropinosomes at the base of a larger ruffle. Membrane relaxes (00:56), small protrusions form with increased AktPH (01:17),  
463 two small ruffles, one in the back and one in the front mergers with the larger ruffle (01:32 -> 01:39) followed by post closure AktPH recruitment  
464 (01:53). Frame rate of 7s and region of 11x9x12  $\mu\text{m}$ .  
465 **Video 8. Corresponds to Fig. 5c.** Isosurface and dual-volumetric intensity projection of mNG-membrane and mSc-AktPH showing a smooth and  
466 relaxed membrane (00:00). A single macropinosome forms (05:06) followed by a large increased in membrane activity (06:35) resulting in a  
467 significant number of macropinosomes, indicated by the post closure AktPH recruitment, that turns into the chaotic membrane structure (06:35  
468 -> 13:18). Frame rate of 8s and region size of 27x22x16  $\mu\text{m}$ .  
469 **Video 9. Corresponds to Fig. 5e.** Side view of mNG-membrane isosurface and mesh membrane with volumetric AktPH (Magenta Hot) shows the  
470 continued AktPH localization within the extending membrane structure (06:35). Utilizing the Magenta-Hot LUT regions displaying in white  
471 represent the increase in AktPH post macropinosome closure signifying a formed macropinosome (05:55; 06:59; 08:12; 11:50). Frame rate of 8s  
472 and region size of 27x22x16  $\mu\text{m}$ .  
473 **Video 10. Corresponds to Fig. 6a, b, c.** CSF-1 starved macrophage displayed using mNG-membrane isosurface/mesh/volume and AktPH volumes  
474 as magenta-hot under the mesh and Magenta alongside the volume membrane. The macrophage was imaged 07:41 prior to stimulation and  
475 reimaged one minute after CSF-1 stimulation (08:41) providing time to ensure instrument and imaging conditions had not changed. The starved  
476 cell ruffled and formed macropinosomes similar to the conventional cells (00:06; 01:46; 03:26) and upon stimulation (08:41) a large circular dorsal  
477 ruffle forms corralling the AktPH to one concentrated spot in the cell (16:22). Frame rate of 6.25s and region size of 49x60  $\mu\text{m}$ .  
478 **Video 11. Corresponds to Fig. 6d.** The brightfield view starts promptly after stimulation showing the majority of macrophages performing the  
479 similar dorsal membrane clearing seen in the LLSM imaging.  
480 **Video 12. Corresponds to Fig. 7a, b. LPS Stimulation.** Isosurface of mNG-Mem and dual-color volumetric intensity projects of mNG-Mem and  
481 mSc-AktPH showing the activity of an LPS treated cell. Initial imaging starts (00:00) with a cluster of membrane rich in AktPH that goes on to  
482 create many macropinosomes as it expands toward the upper right region of the field of view. The activity changes directions toward the upper  
483 left region of the cell and proceeds to move counterclockwise (01:14), over the nucleus and back to the initial location ending at (04:42). Additional  
484 macropinosomes are seen forming on the left region with the increased AktPH flare up post closure (04:42). Finally, several formations occur in  
485 the bottom right of the cell (05:05 – 08:18) many of which go on to merge with one another. Framerate of ~7s and Region of 68x77x21  $\mu\text{m}$ .  
486 **Video 13. Corresponds to Fig. 7c, d. Non-treated control.** Isosurface of mNG-Mem and dual-color volumetric intensity projects of mNG-Mem  
487 and mSc-AktPH showing the imaging of a nontreated cell (10:47). Two AktPH rich regions of membrane ruffling are seen in the bottom right of  
488 the cell (02:17) that form several small macropinosomes, indicated by a spike in AktPH around the formed macropinosome. The cell shows activity  
489 that is representative of the untreated experiments including macropinosome formations, exploration, and overall membrane ruffling. Framerate  
490 of ~6.5s and Region of 68x77x21  $\mu\text{m}$ .  
491

## 492 References

- 493 1 Freeman, S. A. *et al.* Lipid-gated monovalent ion fluxes regulate endocytic traffic and support immune  
494 surveillance. *Science* **367**, 301-305, doi:10.1126/science.aaw9544 (2020).
- 495 2 Bohdanowicz, M. & Grinstein, S. Role of phospholipids in endocytosis, phagocytosis, and macropinocytosis.  
496 *Physiol Rev* **93**, 69-106, doi:10.1152/physrev.00002.2012 (2013).
- 497 3 Doodnauth, S. A., Grinstein, S. & Maxson, M. E. Constitutive and stimulated macropinocytosis in  
498 macrophages: roles in immunity and in the pathogenesis of atherosclerosis. *Philos Trans R Soc Lond B Biol*  
499 *Sci* **374**, 20180147, doi:10.1098/rstb.2018.0147 (2019).
- 500 4 Kerr, M. C. & Teasdale, R. D. Defining macropinocytosis. *Traffic* **10**, 364-371, doi:10.1111/j.1600-  
501 0854.2009.00878.x (2009).
- 502 5 Redka, D. S., Gutschow, M., Grinstein, S. & Canton, J. Differential ability of proinflammatory and anti-  
503 inflammatory macrophages to perform macropinocytosis. *Mol Biol Cell* **29**, 53-65, doi:10.1091/mbc.E17-06-  
504 0419 (2018).
- 505 6 Egami, Y., Taguchi, T., Maekawa, M., Arai, H. & Araki, N. Small GTPases and phosphoinositides in the  
506 regulatory mechanisms of macropinosome formation and maturation. *Front Physiol* **5**, 374,  
507 doi:10.3389/fphys.2014.00374 (2014).
- 508 7 Swanson, J. A. & Yoshida, S. Macropinosomes as units of signal transduction. *Philos Trans R Soc Lond B Biol*  
509 *Sci* **374**, 20180157, doi:10.1098/rstb.2018.0157 (2019).
- 510 8 Yoshida, S. *et al.* Differential signaling during macropinocytosis in response to M-CSF and PMA in  
511 macrophages. *Front Physiol* **6**, 8, doi:10.3389/fphys.2015.00008 (2015).
- 512 9 Lou, J., Low-Nam, S. T., Kerkvliet, J. G. & Hoppe, A. D. Delivery of CSF-1R to the lumen of macropinosomes  
513 promotes its destruction in macrophages. *J Cell Sci* **127**, 5228-5239, doi:10.1242/jcs.154393 (2014).
- 514 10 Bloomfield, G. & Kay, R. R. Uses and abuses of macropinocytosis. *J Cell Sci* **129**, 2697-2705,  
515 doi:10.1242/jcs.176149 (2016).

516 11 Pacitto, R., Gaeta, I., Swanson, J. A. & Yoshida, S. CXCL12-induced macropinocytosis modulates two distinct  
517 pathways to activate mTORC1 in macrophages. *J Leukoc Biol* **101**, 683-692, doi:10.1189/jlb.2A0316-141RR  
518 (2017).

519 12 Condon, N. D. *et al.* Macropinosome formation by tent pole ruffling in macrophages. *J Cell Biol* **217**, 3873-  
520 3885, doi:10.1083/jcb.201804137 (2018).

521 13 Swanson, J. A. Shaping cups into phagosomes and macropinosomes. *Nat Rev Mol Cell Biol* **9**, 639-649,  
522 doi:10.1038/nrm2447 (2008).

523 14 Bohdanowicz, M. *et al.* Phosphatidic acid is required for the constitutive ruffling and macropinocytosis of  
524 phagocytes. *Mol Biol Cell* **24**, 1700-1712, S1701-1707, doi:10.1091/mbc.E12-11-0789 (2013).

525 15 Botelho, R. J. *et al.* Localized biphasic changes in phosphatidylinositol-4,5-bisphosphate at sites of  
526 phagocytosis. *Journal of Cell Biology* **151**, 1353-1367, doi:DOI 10.1083/jcb.151.7.1353 (2000).

527 16 Freeman, S. A. & Grinstein, S. Phagocytosis: receptors, signal integration, and the cytoskeleton. *Immunol*  
528 *Rev* **262**, 193-215, doi:10.1111/imr.12212 (2014).

529 17 Swanson, J. A. & King, J. S. The breadth of macropinocytosis research. *Philos Trans R Soc Lond B Biol Sci* **374**,  
530 20180146, doi:10.1098/rstb.2018.0146 (2019).

531 18 King, J. S. & Kay, R. R. The origins and evolution of macropinocytosis. *Philos Trans R Soc Lond B Biol Sci* **374**,  
532 20180158, doi:10.1098/rstb.2018.0158 (2019).

533 19 Veltman, D. M. *et al.* A plasma membrane template for macropinocytic cups. *Elife* **5**,  
534 doi:10.7554/eLife.20085 (2016).

535 20 Maekawa, M. *et al.* Sequential breakdown of 3-phosphorylated phosphoinositides is essential for the  
536 completion of macropinocytosis. *Proc Natl Acad Sci U S A* **111**, E978-987, doi:10.1073/pnas.1311029111  
537 (2014).

538 21 Araki, N., Egami, Y., Watanabe, Y. & Hatae, T. Phosphoinositide metabolism during membrane ruffling and  
539 macropinosome formation in EGF-stimulated A431 cells. *Exp Cell Res* **313**, 1496-1507,  
540 doi:10.1016/j.yexcr.2007.02.012 (2007).

541 22 Yoshida, S., Hoppe, A. D., Araki, N. & Swanson, J. A. Sequential signaling in plasma-membrane domains  
542 during macropinosome formation in macrophages. *J Cell Sci* **122**, 3250-3261, doi:10.1242/jcs.053207  
543 (2009).

544 23 Welliver, T. P. & Swanson, J. A. A growth factor signaling cascade confined to circular ruffles in macrophages.  
545 *Biol Open* **1**, 754-760, doi:10.1242/bio.20121784 (2012).

546 24 Araki, N., Johnson, M. T. & Swanson, J. A. A role for phosphoinositide 3-kinase in the completion of  
547 macropinocytosis and phagocytosis by macrophages. *J Cell Biol* **135**, 1249-1260,  
548 doi:10.1083/jcb.135.5.1249 (1996).

549 25 Buckley, C. M. & King, J. S. Drinking problems: mechanisms of macropinosome formation and maturation.  
550 *Febs Journal* **284**, 3778-3790, doi:10.1111/febs.14115 (2017).

551 26 Gao, L., Shao, L., Chen, B. C. & Betzig, E. 3D live fluorescence imaging of cellular dynamics using Bessel beam  
552 plane illumination microscopy. *Nat Protoc* **9**, 1083-1101, doi:10.1038/nprot.2014.087 (2014).

553 27 Goddard, T. D. *et al.* UCSF ChimeraX: Meeting modern challenges in visualization and analysis. *Protein Sci*  
554 **27**, 14-25, doi:10.1002/pro.3235 (2018).

555 28 Luyendyk, J. P. *et al.* Genetic analysis of the role of the PI3K-Akt pathway in lipopolysaccharide-induced  
556 cytokine and tissue factor gene expression in monocytes/macrophages. *J Immunol* **180**, 4218-4226, doi:DOI  
557 10.4049/jimmunol.180.6.4218 (2008).

558 29 Stewart, S. A. *et al.* Lentivirus-delivered stable gene silencing by RNAi in primary cells. *RNA* **9**, 493-501,  
559 doi:10.1261/rna.2192803 (2003).

560 30 Sancak, Y. *et al.* The Rag GTPases bind raptor and mediate amino acid signaling to mTORC1. *Science* **320**,  
561 1496-1501, doi:10.1126/science.1157535 (2008).

562 31 Chertkova, A. O. *et al.* Robust and Bright Genetically Encoded Fluorescent Markers for Highlighting  
563 Structures and Compartments in Mammalian Cells. *bioRxiv*, 160374, doi:10.1101/160374 (2020).

564 32 Fejer, G. *et al.* Nontransformed, GM-CSF-dependent macrophage lines are a unique model to study tissue  
565 macrophage functions. *Proc Natl Acad Sci U S A* **110**, E2191-2198, doi:10.1073/pnas.1302877110 (2013).

566 33 Lebedev M, S. P., Kerkvliet JG, Hoppe AD, Thiex N. Immortal fetal liver macrophages as a new model for  
567 studying macrophage function. *Molecular Biology of the Cell* **27** (2016).

568 34 Stanley, E. R., Cifone, M., Heard, P. M. & Defendi, V. Factors regulating macrophage production and growth:  
569 identity of colony-stimulating factor and macrophage growth factor. *J Exp Med* **143**, 631-647,  
570 doi:10.1084/jem.143.3.631 (1976).

571 35 Waheed, A. & Shadduck, R. K. Purification and properties of L cell-derived colony-stimulating factor. *J Lab*  
572 *Clin Med* **94**, 180-193 (1979).

573 36 Chen, B. C. *et al.* Lattice light-sheet microscopy: imaging molecules to embryos at high spatiotemporal  
574 resolution. *Science* **346**, 1257998, doi:10.1126/science.1257998 (2014).

575 37 Lambert, T. & Shao, L. tlambert03/LLSpy: v0.4.8. doi:http://doi.org/10.5281/zenodo.3554482 (2019).

# Figures

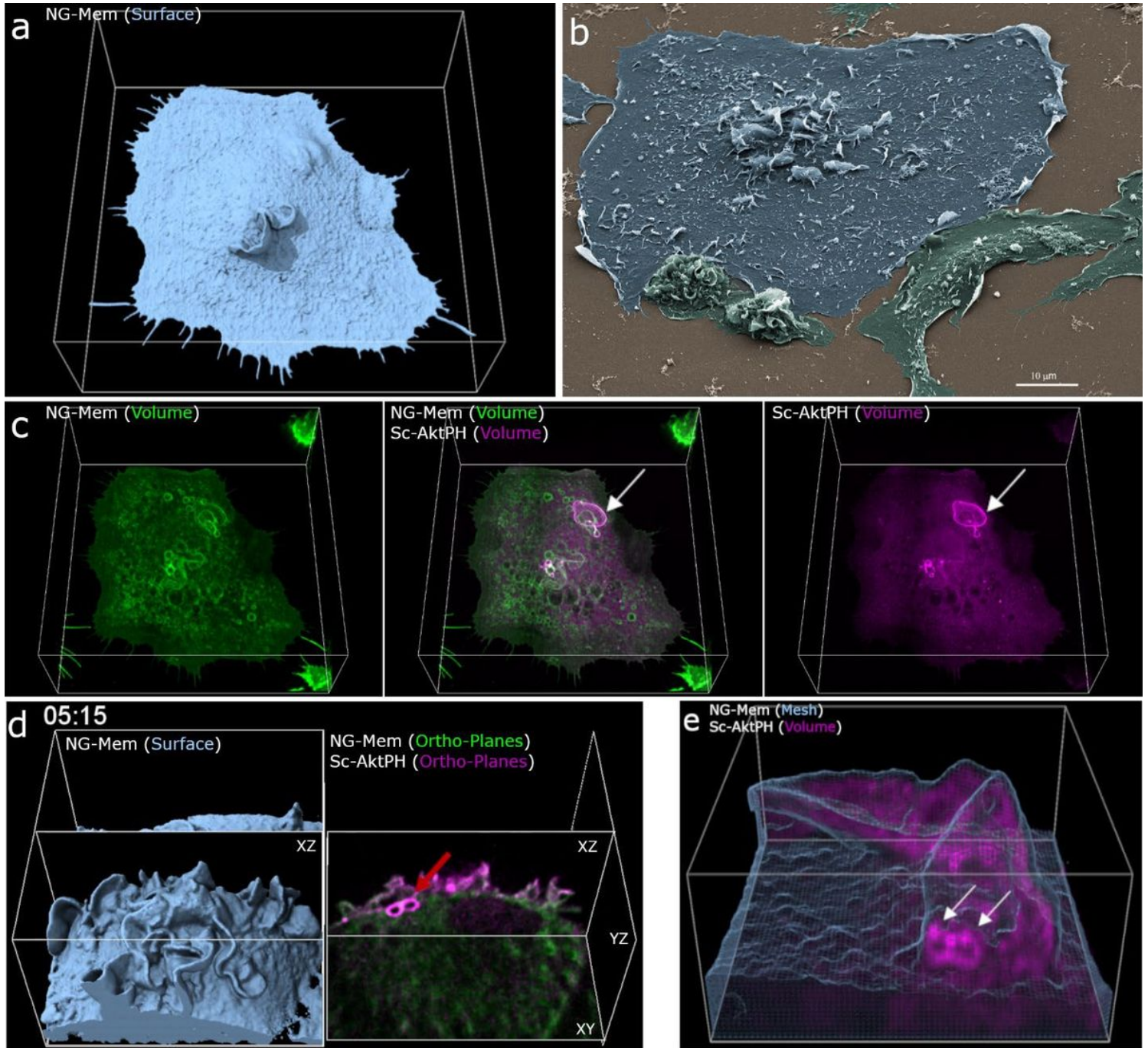


**Figure 1**

3D visualization of macrophages allows insight into membrane structure and phosphatidylinositol dynamics during macropinocytosis. a) Isosurfaces show the plasma membrane of a live cell that is actively macropinocytosing. Region  $68 \times 72 \times 25 \mu\text{m}$  (x, y, z). b) SEM image of a macrophage acutely stimulated with CSF-1 shows high-resolution fixed cells. Scale bar is  $10 \mu\text{m}$ . c) Volumetric intensities show specific local fluorescence (left-to-right) volumetric membrane (green), dual volumetric membrane and mSc-AktPH, volumetric mSc-AktPH (magenta). Volumetric renderings provide a method to visualize

the transient fluorescent intensities throughout the volume of the cell. Region is 68x72x25  $\mu\text{m}$ . d) Combinations of visualization techniques such as Isosurface (left) displayed alongside orthogonal planes (right) further clarify how each 360 plane is chosen to show internal intensities. Region of 29x30x19  $\mu\text{m}$ . e) Mesh rendering of the mNG-membrane probe along with volumetric mSc-AktPH provides a representation of the plasma membrane structure as well as underlying fluorescence. The white arrows indicate the post closure recruitment of mSc-AktPH. Region 13x14x7  $\mu\text{m}$ . Different rendering methods provide insight into cellular characteristics such as structure, depth, and fluorescent intensity and provide a foundation for visualizing localization of mSc-AktPH to the constantly changing plasma membrane during macropinocytosis.

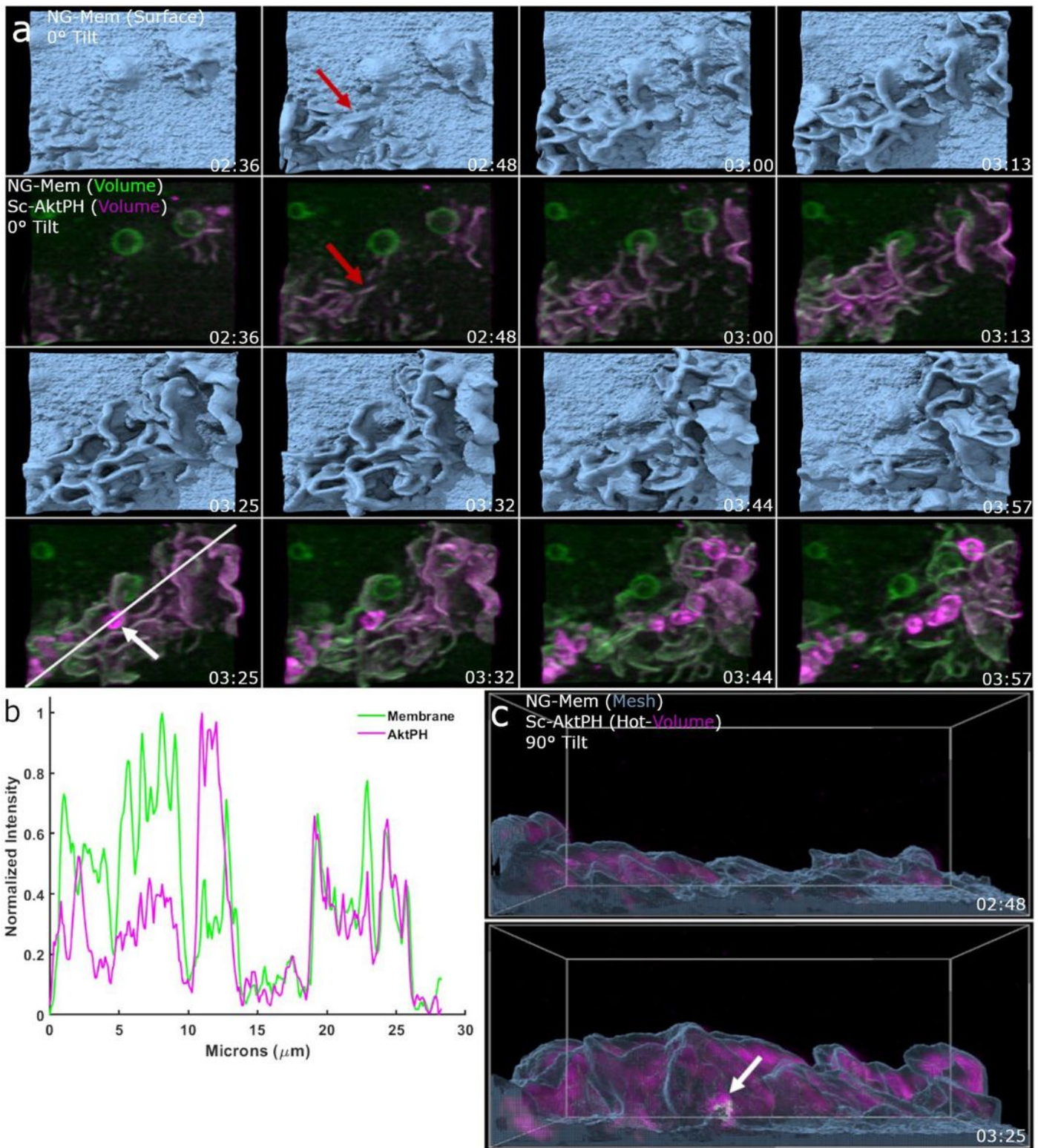


**Figure 2**

Early PI3K activity leads to amplification of PIP3/PIP2 in developing ruffles, macropinosome formation, and post closure recruitment. a) Top view of an mNG-mem isosurface rendering provides depth for 3D visualization of ruffle extension. Dual-color volumetric intensity display comparing the recruitment of mSc-AktPH to early and expanding ruffles as well as sealed macropinosomes (Region 21x19 $\mu\text{m}$ ). b) Intensity line-scan of the volumetric mNG-Mem and mSc-AktPH shows their relative intensities for

extending membrane ruffles, as well as recruitment around a sealed macropinosome. c) Side view of the isosurface mesh plasma membrane and volumetric mSc-AktPH (Magenta Hot color scale) from a shows that the early stages of ruffle development is filled with mSc-AktPH and the resulting macropinosome (white arrow) receives a final intense mSc-AktPH recruitment around the formed macropinosome at the bottom of the ruffle. Region of 21x19x15um.

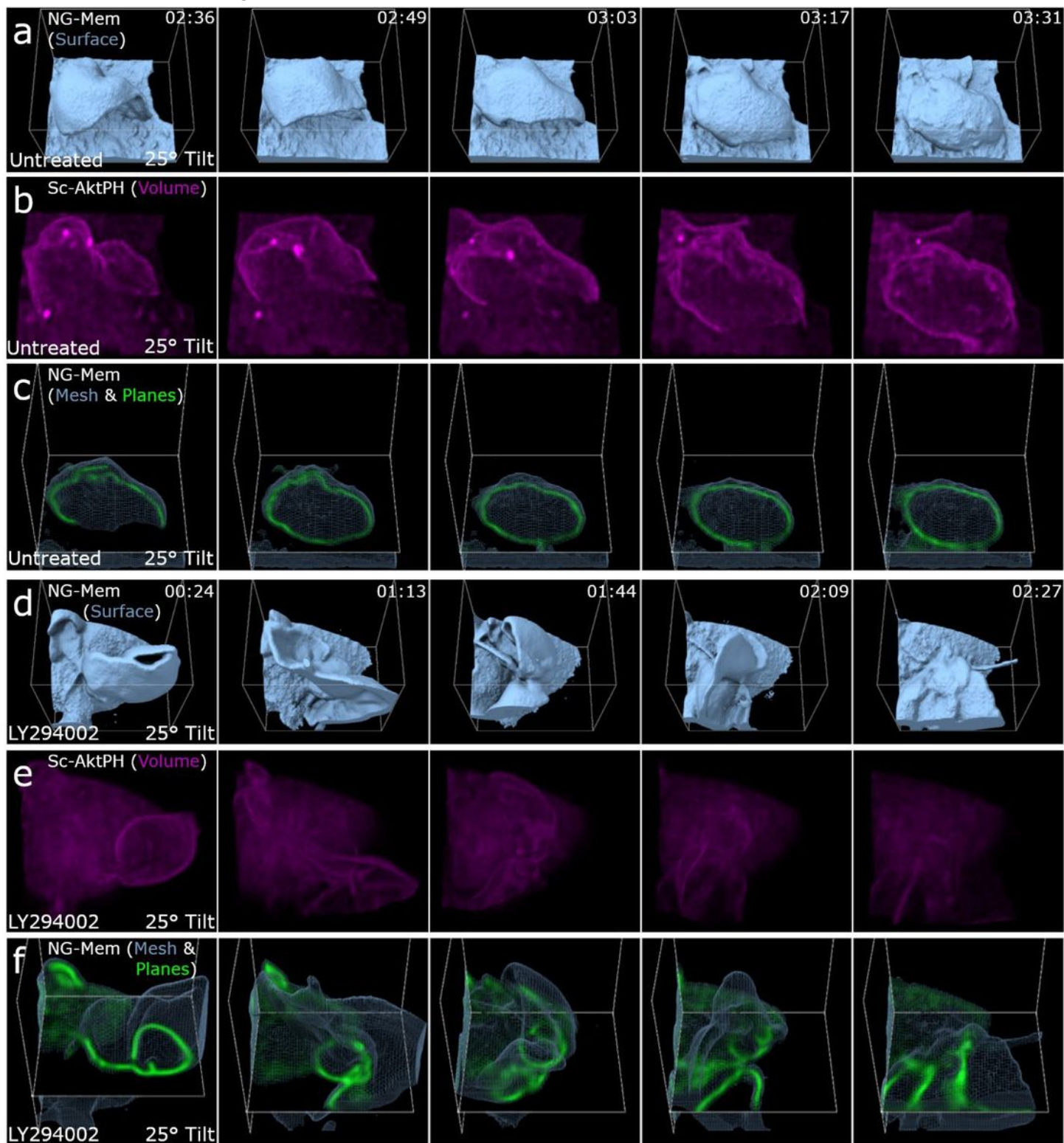


Figure 3

PI3K activity is required for membrane sealing and separation from PM/internalization of a complete macropinosome but not membrane ruffling a) Isosurface rendering of mNG-mem for an untreated macrophage during a successful macropinocytosis event where the sheet curls back toward the membrane for fusion/sealing. Region 12x13x10  $\mu\text{m}$ ;m b) Volumetric rendering of Sc-AktPH of the untreated cell shows the increase of PI3K activity in the ruffle that creates a macropinosome. 12x13x10  $\mu\text{m}$ ;m c) Mesh and orthogonal planes of mNG-mem show the internal membrane organization of the ruffle and resulting macropinosome. 12x13x10  $\mu\text{m}$ ;m d) Isosurface rendering of an LY294002 treated macrophage provides depth to the attempted closure of a macropinocytic cup. Region 10x12x10  $\mu\text{m}$ ;m. e) Volumetric intensity rendering of Sc-AktPH for an LY294002-treated macrophage shows the diffuse distribution of AktPH and minimal PI3K activity. The cytosolic intensities were co-scaled for the untreated and treated macrophage. Region 10x12x10  $\mu\text{m}$ ;m f) XY-plane for the mNG-mem probe of an LY294002-treated cell during a failed macropinocytosis event. In the surface view, the ruffle appeared to form a macropinosome; however, when overlaid with the plane view is became clear that it failed to fully form into a macropinosome. The ruffle quickly reduced in size and became undistinguishable within the cytosol, while never receiving the post closure increase of PI3K activity. Region 10x12x10  $\mu\text{m}$ ;m.

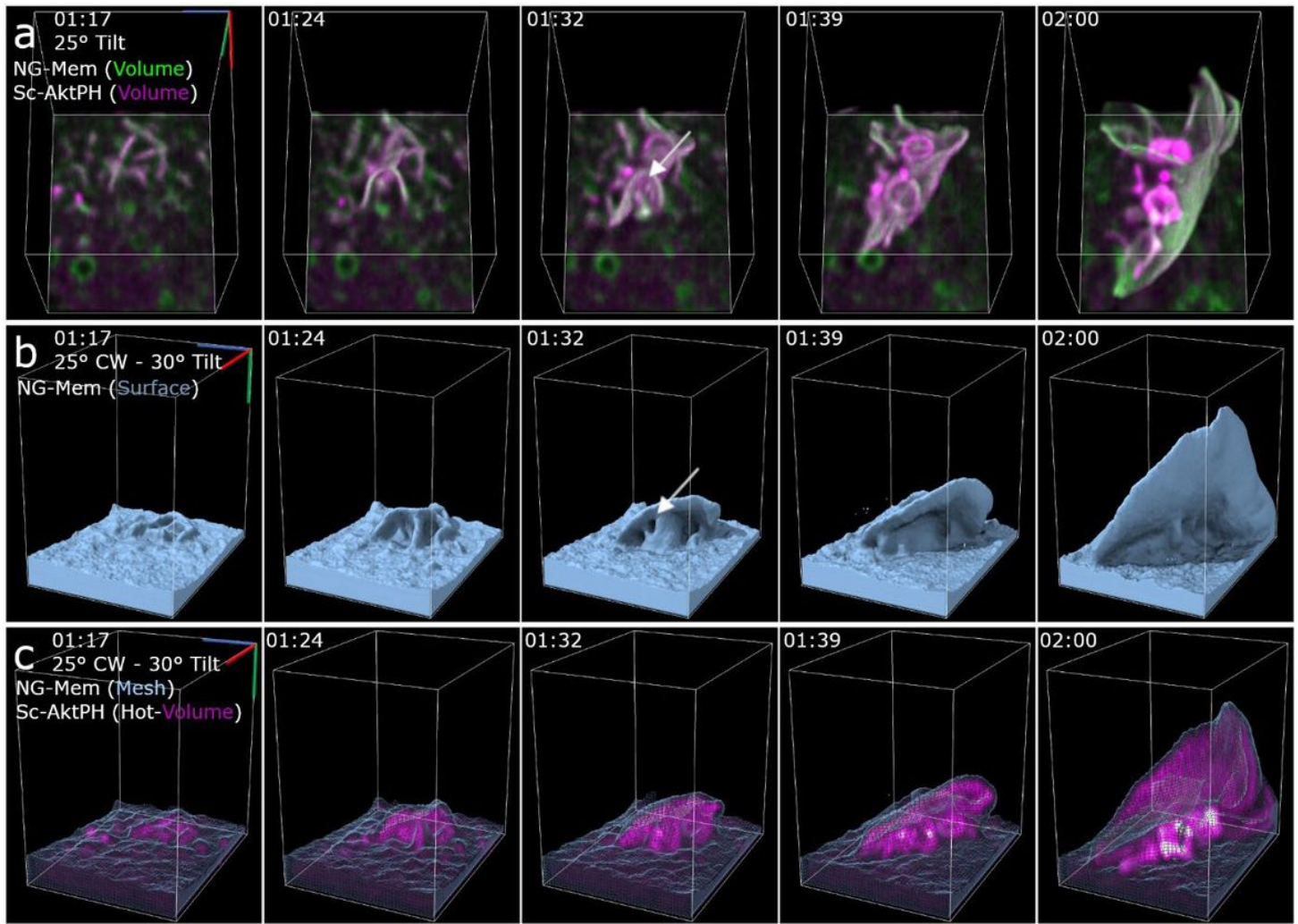


Figure 4

Macropinosomes form via PI3K-primed ruffle fusion. a) Dual volumetric intensities of mNG-mem and mSc-AktPH show the intensity of each probe as the ruffles and macropinosomes form. The montage shows the earliest stage of the ruffle that extends vertically and forms macropinosomes along the length near the base of the primary ruffle as a result of smaller mSc-AktPH-rich extensions colliding. The white arrow points at the macropinosome forming region further emphasized in the isosurface. Region 9x12x13  $\mu\text{m}$ . b) Isosurface rendering of mNG-membrane shows the structure of the extending ruffle and the continued sheet extension after the macropinosomes formed. The white arrow emphasizes the small pocket that closes to form one of the macropinosomes. Region 9x12x13  $\mu\text{m}$ . c) Mesh surface rendering of mNG-mem and volumetric mSc-AktPH shows the internalized macropinosome with the increased localization of mSc-AktPH at the bottom of the ruffle. Region 11x9x12  $\mu\text{m}$ .

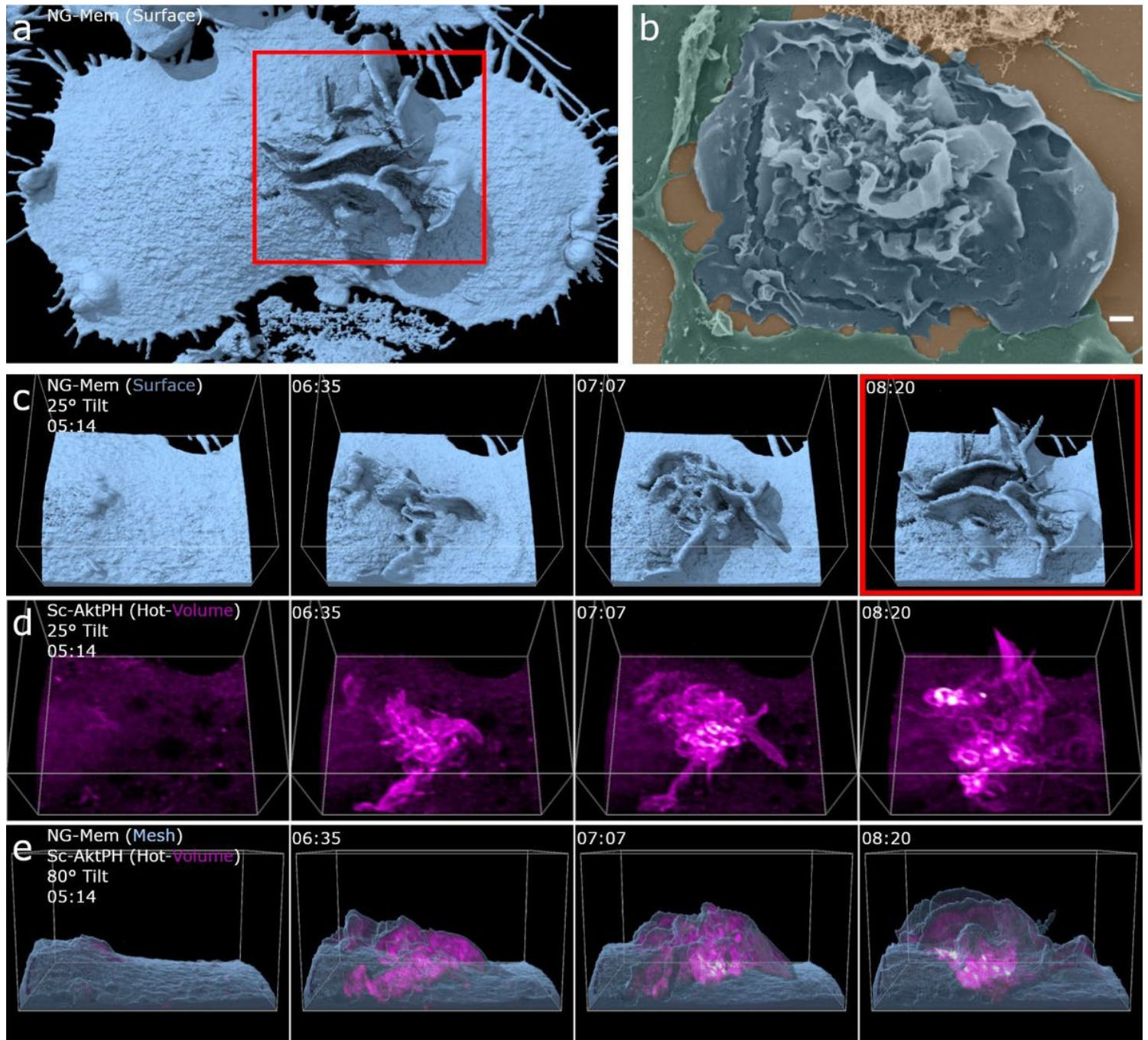
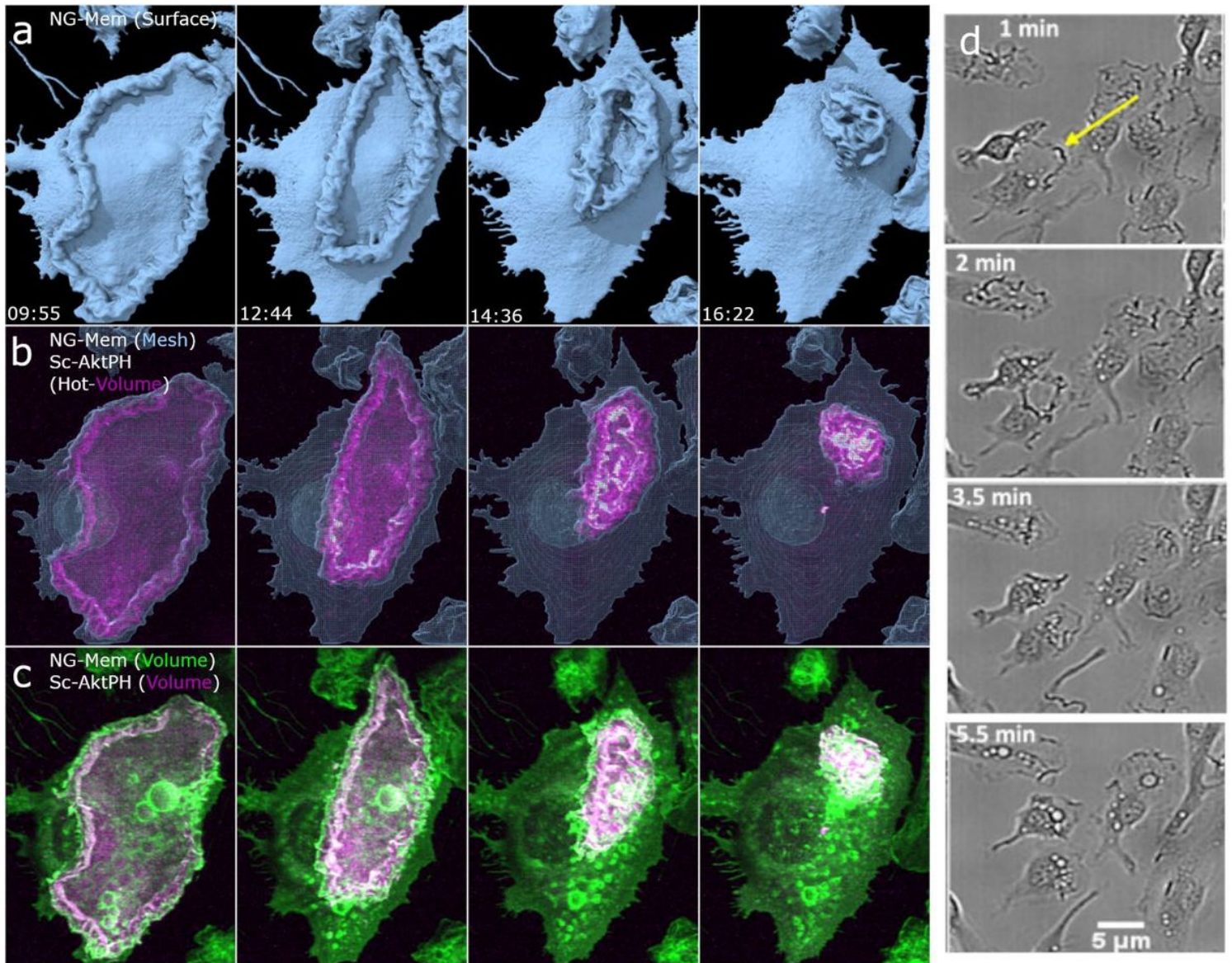


Figure 5

Phosphatidylinositol localization and chaotic ruffling underlie macropinocytosis in complex membrane structures. a) Single time point, full cell surface rendering of chaotic macropinocytosis event. The red box correlates to the same frame in c-d. b) SEM images of a BMDM showing similar highly active ruffling regions c) Isosurface montage shows the chaotic orientation of membrane structure. Region 27x22x16  $\mu\text{m}$ , 25° tilt. d) Volumetric AktPH (Magenta-Hot) provides a more detailed emphasis on the AktPH activity within the membrane ruffles and highlights the macropinosomes that have formed. Region 27x22x16  $\mu\text{m}$  with a 25° tilted view. e) Mesh Surface with AktPH (Magenta Hot) shows the AktPH activity as the ruffle develops as well as the increased recruitment around formed macropinosomes at the base of the event.



**Figure 6**

Growth factor starvation and stimulation results in the formation of large circular dorsal ruffles that corral PIP3/PIP2. Macrophages were starved of CSF-1 for 24 h, imaged for 5 minutes as a baseline, and imaging restarted 1 min after stimulation with 50 ng·mL<sup>-1</sup> CSF-1. Four-frame montages provide a visual display of the large dorsal ruffle that acts as a diffusional barrier that restricts PIP3/PIP2 to the inside of the ruffle as it is cleared from the surface. This barrier is likely acting as a signal amplification

mechanism stimulating the production of many macropinosomes. a) Isosurface rendering provides crisp surface directionality, b) Surface mesh and volumetric AktPH (magenta-hot), show the restricted probe as the membrane converges c) Volumetric Intensity of both mNG-Membrane and mSc-AktPH show the intensity locations of the membrane ruffle and the restricted AktPH. 49x60  $\mu\text{m}$  d) Bright field images showing multiple cells responding to stimulation with similar dorsal membrane clearing.

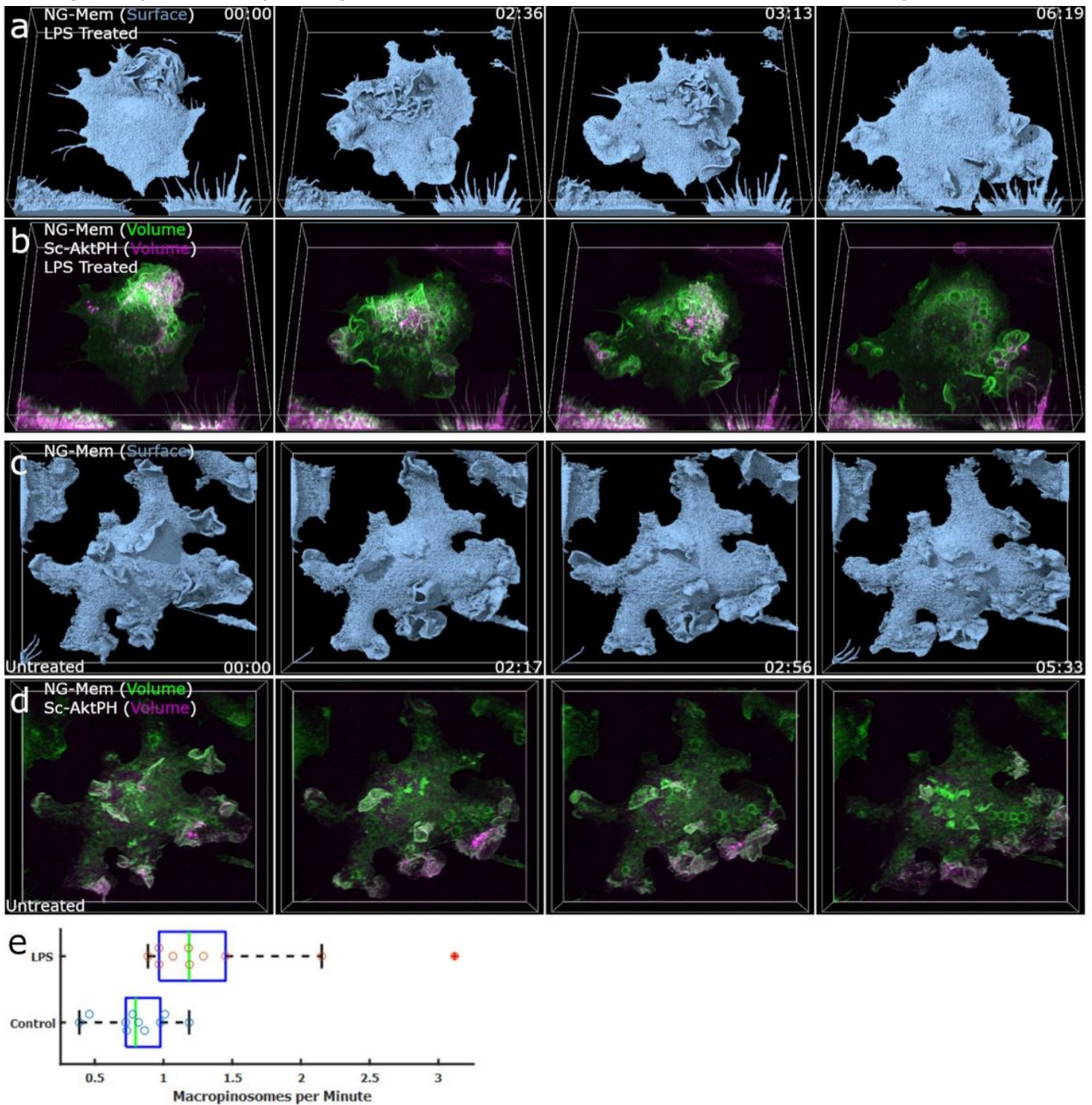


Figure 7

LPS stimulation increases membrane ruffling and macropinocytosis. Macrophages were pretreated with 100 ng·ml<sup>-1</sup> LPS for 24 h prior to imaging. a) Surface rendering of mNG-Mem on an LPS stimulated macrophage provides a surface level understanding of the membrane, exploration, ruffling, and PM structure. b) Dual-color volumetric intensity projections of mNG-Mem and mSc-AktPH for an LPS stimulated cell provided the intensity activity during increased macrophage activity and shows the highly AktPH rich regions of membrane ruffling. Region 68x77x21  $\mu\text{m}$  c) Untreated macrophage Isosurface showing visibly less exploratory behavior. d) Dual-color volumetric intensity rendering of the untreated macrophage gives insight on the AktPH activity inside of the cell during macropinocytosis and allows for the quantitative comparison of macropinosomes formed between the stimulated and unstimulated cells. Region 68x77x21  $\mu\text{m}$ . e) Box plot showing the difference in macropinocytic activity between untreated and LPS treated macrophages. All macropinosomes greater than 1  $\mu\text{m}$  were manually counted using a z-projection MIP in Fiji and were distinguished by the post closure spike in mSc-AktPH intensity.

## Supplementary Files

This is a list of supplementary files associated with this preprint. Click to download.

- [Vid1Fig1ACVolumeSurfaceTimeStamped.avi](#)
- [Vid2Fig1DXPlaneScanTimeStamped.avi](#)
- [Vid3Fig2ASurfVolTimeStamped.avi](#)
- [Vid4Fig2CMeshVolTimeStampedWithPause.avi](#)
- [Vid5Fig3CostitComparisonTimeStamped.avi](#)
- [Vid6Fig3LYSurfVolSplitTimeStamped.avi](#)
- [Vid7Fig4SurfSplitVolumesTimeStamped.avi](#)
- [Vid8Fig5CDChaosSurfVolsTimeStamped.avi](#)
- [Vid9Fig5CEChaosSurfMeshVolTimeStamped.avi](#)
- [Vid10Fig6ABCCSFFullTimeStamped.avi](#)
- [Vid11Fig6DCSFBrightField.avi](#)
- [Vid12Fig7ABLPSClusterTimeStamped.avi](#)
- [Vid13Fig7BLPSUntreatedComparisonTimeStamped.avi](#)